ANNUAL REVIEWS

Annual Review of Nuclear and Particle Science

New Results on Short-Range Correlations in Nuclei

Nadia Fomin,[1] Douglas Higinbotham,[2] Misak Sargsian,[3] and Patricia Solvignon[4]

[1]Department of Physics and Astronomy, University of Tennessee, Knoxville, Tennessee 37996
[2]Thomas Jefferson National Accelerator Facility, Newport News, Virginia 23606
[3]Department of Physics, Florida International University, Miami, Florida 33199
[4]Department of Physics, University of New Hampshire, Durham, New Hampshire 03824

Annu. Rev. Nucl. Part. Sci. 2017. 67:129–59

First published as a Review in Advance on July 31, 2017

The *Annual Review of Nuclear and Particle Science* is online at nucl.annualreviews.org

https://doi.org/10.1146/annurev-nucl-102115-044939

Keywords

short-range nucleon correlations, high-energy electron–nucleus scattering, deep-inelastic nuclear scattering, superfast quarks

Abstract

Nuclear dynamics at short distances is one of the most fascinating topics of strong interaction physics. The physics of it is closely related to the understanding of the role of the QCD in generating nuclear forces at short distances, as well as of the dynamics of the superdense cold nuclear matter relevant to the interior of neutron stars. The emergence of high-energy electron and proton beams has led to significant recent progress in high-energy nuclear scattering experiments investigating the short-range structure of nuclei. These experiments, in turn, have stimulated new theoretical studies resulting in the observation of several new phenomena specific to the short-range structure of nuclei. We review recent theoretical and experimental progress in studies of short-range correlations in nuclei and discuss their importance for advancing our understanding of the dynamics of nuclear interactions at short distances.

Contents

1. INTRODUCTION

1.1. Nuclear Physics at Short Distances

One of the outstanding issues in contemporary nuclear physics is understanding the role of quantum chromodynamics (QCD) in generating the nuclear forces. There has been significant progress in understanding the medium- to long-range part ($\gtrsim$1.2 fm) of the nuclear forces in terms of effective field theories in which pion exchange forces are constructed to satisfy QCD symmetries and the dynamics in which the pion is a Goldstone boson of the spontaneously broken chiral symmetry (for a recent review, see Reference 1). However, one of the challenging and less well understood domains of nuclear forces is that of intermediate to short distances ($\lesssim$1.2 fm). This is the domain of the transition from baryonic to quark–gluon degrees of freedom, where one expects a host of new phenomena inherent to QCD dynamics that are not visible to long-range nuclear forces. These include chiral symmetry, quark interchanges, gluon dynamics, and hidden color states, among others. One of the most fascinating short-distance phenomena is the practically unexplored dynamics of the nuclear repulsive core. We literally owe our existence to the nuclear core, without which nuclei would collapse to sizes $\leq$0.3–0.4 fm, followed by the onset of quark–gluon degrees of freedom and restoration of chiral symmetry with unimaginable consequences for the order of the Universe as we know it.

Within the above-mentioned effective field theories, the short-range nuclear forces are described through the effective contact interactions whose internal structure is invisible in low-energy

processes. However, in high-momentum-transfer processes the dynamical content of these contact interactions is increasingly important, and this review addresses recent progress in these studies. From the nuclear physics point of view, this region is dominated by short-range multinucleon correlations. Our understanding of the dynamics of these correlations is relevant not only to the QCD dynamics of the nuclear forces but also to the physics of high-density nuclear matter that one expects to exist at the cores of neutron stars.

1.2. Importance of Short-Range Correlations

The atomic nucleus, as a bound system of interacting fermions in which the Hamiltonian does not commute with the momentum operator, gives rise to the phenomenon of momentum distribution of its constituents. Fermi statistics, along with the fact that the combined volume of A nucleons is comparable to the nuclear volume, makes the effect of the nucleon correlations a phenomenon that ranges from long to short distances. Long-range correlations have been reasonably well studied experimentally and have been understood on the basis of Pauli blocking effects and the long-range part of the nuclear forces (2). Short-range nucleon correlations, by contrast, represent the most intriguing part of the nuclear dynamics; experimental studies in this area are intensifying with the emergence of high-energy accelerators capable of performing nuclear experiments with high-intensity beams, allowing for precision measurements of small cross sections.

Historically, the importance of short-range correlations (SRCs) was first emphasized by Jastrow (3), who observed that the application of variational methods to estimate the upper limit of the ground-state energy fails for the strong interaction, whose range, r_0, is comparable with the size of the nucleon. In this case, the expectation value of the mean potential energy per nucleon is $\bar{V} = (Nr_0^3/\Omega) \mid V_0 \mid$, where Ω is the nuclear volume and V_0 is the average potential of the nucleon–nucleon (NN) interaction at $r \leq r_0$. From this relation, one observes that in the hard sphere limit of the NN interaction core, the upper bound of the ground-state energy increases without limit. This problem was solved (3) through the introduction of NN correlations at $r \leq r_0$ distances based on the cluster decomposition approach and the choice of an ad hoc form for the correlation function. Although this approach solved the ground-state energy problem, it did not address the dynamical origin of such correlations. At about the same time, correlation functions were introduced within the framework of the Brueckner–Goldstone theory (for a review and relevant references, see Reference 4), in which the nucleon's finite size introduced a positional correlation that modified the independent particle-state wave function.

An approach that demonstrated how the dynamical property of strong forces at short distances enters into SRCs (5) involves obtaining the asymptotic solution of the N-body Schrödinger equation in the large-momentum limit of the bound nucleons. In this case, for specific behavior of the NN potential at short distances (see Section 2.1, below), the momentum distribution of high-momentum nucleons is defined as $n(p) \sim [\mid V(p) \mid^2]/p^4$. This relation indicates that probing the large momentum of the bound nucleon in the nucleus allows one to access the NN potential at large relative momenta or small relative distances. This approach defines the main strategy of SRC studies, which is accessing the dynamics of NN interactions at short distances by probing bound nucleons with large initial momentum and removal energy. Note that the observation of the relation between short-distance phenomena in the nucleus and the high-momentum component of the nuclear wave function had already been made within the Brueckner–Goldstone theory (see, e.g., Reference 6); however, the analytic property of the NN potential for which the high-momentum component would have the above-presented form was not identified.

Another issue that SRC studies aim to address is the existence of three-nucleon ($3N$) and possibly higher-order correlations. The questions in this case are whether SRCs of more than two nucleons can be formed and what the necessary conditions are to generate deeply bound

high-momentum nucleons. These studies have significant astrophysical importance for understanding the dynamics of the superdense nuclear matter that is formed in the core of neutron stars.

Finally, a new direction in SRC studies involves the QCD content of these high-density fluctuations. Recent experiments have begun to probe quark distributions in the kinematic region in which single quarks carry momentum larger than that of the individual nucleon and are referred to as superfast quarks.

1.3. Experiments with High-Energy and High-Intensity Beams

As introduced above, the main experimental methodology of accessing SRCs is to probe a deeply bound nucleon in the nucleus with large momentum and removal energy. To realize such a possibility, one needs processes in which the energy transferred to the nucleon in the SRC significantly exceeds the potential and kinetic energies characteristic of the SRC. Such an instantaneous removal of the deeply bound nucleon from the SRC will release correlated nucleons, the detection of which would provide an additional window into the dynamics of SRCs in the nucleus.

Such experiments are possible only with high-energy probes. The first possibility presented itself at Stanford Linear Accelerator Center (SLAC), where electron beams with energy up to 20 GeV enabled unprecedented measurements of inclusive $A(e,e')X$ processes in the kinematic region dominated by SRCs (7–11). These experiments permitted, for the first time, access to the high-momentum component of the nuclear wave function through the y-scaling analysis (12). Subsequently, a study (13) of the ratios of inclusive cross sections of nuclei A to the deuteron revealed the first signatures of NN SRCs in the form of the scaling as a function of the Bjorken variable x in the region $1 < x < 2$.

Meanwhile, attempts were made to extend SRC studies to semi-inclusive processes in which knockout protons, or the protons emerging from the NN SRCs as spectators, were detected in coincidence with the scattered electrons (14–17). These experiments unambiguously observed SRC signatures in the form of correlations between missing energy and missing momentum (15) or through the shifts of the scattered electron spectra proportional to the energy and angle of the spectator protons (16, 17). However, such signatures are present for any two-body currents, and due to the restricted magnitudes of the transferred energy and momentum, it was impossible to dynamically suppress the soft two-body processes not related to SRCs (such as meson exchange currents).

The situation changed completely following the construction of the Continuous Electron Beam Accelerator Facility's (CEBAF's) 6-GeV continuous electron beam at Jefferson Lab (JLab), where practically all of the major advances in SRC studies have been made. JLab's high energies, along with the high intensities of the electron beam, enabled precision measurements of the small cross sections characteristic of SRC dynamics in electroproduction reactions. Additionally, triple coincidence experiments were carried out in which additional nucleons were detected: One was struck from the SRC by a virtual photon, and the other emerged as a spectator from the same SRC. Note that at about the same time as JLab experiments were producing initial results, SRC studies were also being performed at Brookhaven National Laboratory (BNL). In the BNL experiments, the Alternating Gradient Synchrotron (AGS) was used as a source of high-energy proton beams (6–15 GeV/c) to perform double $A(p,2p)X$ and triple $A(p,2pn)X$ coincidence experiments aimed at SRC studies. Measurements of both electron–nucleus (eA) and proton–nucleus (pA) experiments were remarkable as they yielded almost identical results for the dynamics of SRCs, thereby confirming the universal nature of the object they were probing in the nucleus.

These experiments further stimulated theoretical research on SRCs, covering issues related to high-energy electron–nucleon processes, modeling high-momentum components of the nuclear wave function, and improving our understanding of both the dominance of the proton–neutron (pn) component of the SRCs and the role of the SRCs in medium modification of the bound

nucleons. These activities, together with recent results from experimental studies of SRCs, are the subject of this review.

1.4. Summary of Recent Progress

Recent experiments studying high-energy *eA* and *pA* processes (18–24) have greatly improved our understanding of the dynamics of *NN* SRCs in nuclei. The new generation of inclusive $A(e,e')X$ experiments (18–20) confirmed the observation made from the analysis of SLAC data (13, 25) that the ratios of nuclear to deuteron cross sections scale in the kinematic region dominated by the scattering from the *NN* SRC. The ratios, designated by the parameter $a_2(A, Z)$, which is directly related to the SRC strength in the high-momentum component of nuclear wave functions, were measured for a wide range of nuclei.

An analysis of the $A(e,e')X$ data in the deep-inelastic region at JLab yielded EMC ratios (see Section 3.2) that characterize the extent of medium modification of partonic distributions of the bound nucleon (26). A comparison between the strengths of the EMC ratios and the $a_2(A, Z)$ parameters revealed an apparent correlation between these two observables (27, 28), strongly suggesting that the medium modification effect is related to the probability of nucleons being in SRCs.

The final group of SRC experiments consisted of high-energy, semi-inclusive triple coincidence measurements (21, 23) that successfully probed the isospin composition of *NN* SRCs in the relative momentum range of ~250–650 MeV/*c*. These experiments observed a strong (by a factor of 20) dominance of *pn* SRCs in nuclei compared with proton–proton (*pp*) and neutron–neutron (*nn*) correlations. Such an excess is understood (21, 29, 30) on the basis of the dominance of the tensor forces in the *NN* interaction at the above-mentioned momentum range corresponding to the average internucleon separation of ~1.1 fm.

The observation of the strong dominance of *pn* SRCs led to the prediction (31, 32) that single proton or neutron momentum distributions in the *NN* SRC domain are inversely proportional to their relative fractions in nuclei. This prediction agrees with the results of variational Monte Carlo (VMC) calculations of the momentum distributions of light nuclei (33), as well as with the SRC model calculation for medium to heavy nuclei (34). Recent experimental verification of *pn* dominance in heavy nuclei (up to ^{208}Pb) (24) provides strong evidence for the universality of this prediction across nuclei.

The isosinglet *pn* dominance in the SRC region makes dedicated studies of the high-momentum component of the deuteron wave function a priority. The first experiment probing the deuteron at large internal momenta was recently completed at JLab (35). Here, the exclusive $d(e,e'p)n$ cross section was measured at unprecedentedly large Q^2 values of 3.5 GeV^2. This experiment succeeded, for the first time, in measuring the deuteron momentum distribution for energies up to 550 MeV/*c* with negligible and controlled effects due to long-range nuclear phenomena and final-state interactions. This experiment will be extended to even more extreme kinematics with the upgraded 12-GeV JLab accelerator. The experimental progress summarized above has stimulated strong theoretical activity in understanding the dynamical origin of SRCs and their implications in the different nuclear phenomena, including the EMC effect, symmetry energy, and the nuclear contact (36–45).

2. RECENT ADVANCES IN THEORY

2.1. Emergence of Short-Range Correlations in Strongly Interacting Fermi Systems

Although Jastrow (3) discussed the correlation picture of multinucleon systems within the cluster development approach, his paper did not address the dynamical origin of the correlations. This topic was discussed in Reference 5, which showed that in the limit of very large internal momenta

of the bound nucleon, the solution of the Lippmann–Schwinger equation is defined at large relative momentum of the pairwise *NN* interaction potential. However, this paper did not discuss whether *NN* correlations will dominate the high-momentum component of the nuclear wave function relative to the higher-order (more than *NN*) correlations. Subsequent studies (46) analyzed the issue of hierarchy of *NN* correlations and observed that if the *NN* potential is a finite-range potential and, in the high-momentum ($q \gg m_N$) limit, behaves as $V(q) \sim (1/q^n)$ (where $n > 1$), then the wave function of the multinucleon system in the limit where one of the nucleons has high momentum is dominated mainly by *NN* correlations.

The emergence of *NN* SRCs can be observed if one considers the Lippmann–Schwinger equation for a bound system with A nucleons interacting through the finite-range pairwise *NN* interactions, $V_{i,j}$, in the form

$$\phi_A(k_1, \cdots k_n, \cdots k_A) = \frac{-\frac{1}{2}\sum_{i\neq j} V_{ij}(q)\phi_A(k_1, \ldots, k_i + q, \ldots, k_j - q, \ldots, k_A)\frac{d^3q}{(2\pi)^3}}{\sum_{i=1}^{A}\frac{k_i^2}{2m_N} - E_B}; \qquad 1.$$

this equation can be used in the iteration approach to calculate the full nuclear wave function. If one starts with the first iteration using the mean-field nuclear wave function on the right-hand side of the equation and considers one of the bound nucleons (say, j) on the left-hand side to have momentum p such that $(p^2/2m_N) \gg E_B$, one observes that the integral on the right-hand side will be dominated by the configuration in which $\mathbf{q} \approx \mathbf{p}$, such that $\mathbf{k_j} - \mathbf{q} \approx \mathbf{0}$, and $\mathbf{k_i} \approx -\mathbf{k_j} \approx -\mathbf{p}$, such that $k_i + q \approx 0$. This situation results in a *NN* correlation with large relative momentum such that (5)

$$\phi_A^{(1)}(k_1, \ldots, k_i = p, \ldots, k_j \approx -p, \ldots, k_A) \sim \frac{V_{NN}(p)}{p^2} f(k_1, \ldots' \ldots' \cdots k_A), \qquad 2.$$

where $f(\cdots)$ is a smooth function of the momenta of noncorrelated nucleons that do not contain momenta k_i and k_j. However, this result does not yet guarantee the dominance of *NN* correlations in the high-momentum part of the nuclear wave function. For that to occur, the higher-order correlations should be parametrically small. In the approximation of pairwise interactions, the higher-order correlations correspond to the higher-order iterations. For example, 3*N* SRCs can be estimated by inserting Equation 2 into Equation 1, yielding

$$\phi_A^{(2)}(\cdots p, \cdots) \sim \frac{1}{p^2}\int \frac{V_{NN}(q)V_{NN}(p)}{(p-q)^2} d^3q. \qquad 3.$$

If one now assumes analytic behavior for the *NN* potential of the form $V_{NN}(q) \sim q^{-n}$ in the large-q limit, then one estimates the parametric dependence of the wave function due to 3*N* SRCs as

$$\phi_A^{(2)}(\cdots p, \cdots) \sim \frac{V(p)}{p^2}\int_{q_{\min}}^{\infty} \frac{dq}{q^n}, \qquad 4.$$

where $q_{\min}$ arises from the finite range of the potential. This relation indicates that for the finite-range interaction with $n > 1$, the second (as well as higher-order) correlation will be parametrically suppressed (21, 25). An important feature of this result is that one will arrive at the same conclusion in the relativistic framework if the nuclear dynamics are described within light-front or Weinberg-type equations for the bound systems (e.g., 46, 47).

The above discussion allows us to conclude that bound systems interacting through pairwise Yukawa-type interactions will generate correlations dominated by *NN* SRCs. Higher-order correlations are possible, but they are parametrically suppressed relative to *NN* SRCs.

To access such correlations experimentally, one needs to probe bound nucleons with high initial momenta, requiring $(p^2/2m_N) \gg E_B$. If such conditions are met, then the asymptotic form

of Equation 2 leads to the following approximate relation for a nucleon momentum distribution at $p > k_F$ (where k_F is the characteristic Fermi momentum of the nucleus):

$$n^A(p) \sim a_{NN}(A) \cdot n_{NN}(p), \quad 5.$$

where the full momentum distribution is normalized as $\int n^A(p)d^3p = 1$. The parameter $a_{NN}(A)$ can be interpreted as a probability of finding a *NN* SRC in the given nucleus *A*. The function $n_{NN}(p)$ is the momentum distribution in the *NN* SRC.

2.2. Conceptual Issues in High-Energy Nuclear Theory

The above discussion indicates that probing the short-distance correlation structure of the nucleus requires probing a bound nucleon with momentum significantly exceeding the characteristic Fermi momentum, $k_F \sim 250$ MeV/*c*. For such a nucleon to be instantaneously removed from the nucleus, the momentum, q, transferred to the bound nucleon should be sufficiently large: $q \gg 2k_F$. Another restriction on the momentum transfer follows from the dynamic picture of SRCs, in which the correlated nucleons have large and comparable momenta in opposite directions. Therefore, in order to unambiguously discriminate the struck nucleon in the final state (p_f) with momentum $\mathbf{p_f} = \mathbf{p_i} + \mathbf{q}$ from the correlated spectator nucleon (p_s), one needs to satisfy the following condition:

$$q \sim p_f \gg p_s \sim 300\text{–}1{,}000 \text{ MeV}/c. \quad 6.$$

Requiring that the interaction off the bound nucleon be quasi-elastic allows us to determine $\mathbf{p_i}$ and leads to the kinematic threshold of $Q^2 = \mathbf{q}^2 - q_0^2 > m_N^2$. Thus, one arrives at the optimal kinematics for probing the SRC structure of nuclei as

$$Q^2 > m_N^2, \quad q \sim p_f \geq \text{few GeV}/c, \quad p_s \sim \text{few hundred MeV}/c. \quad 7.$$

These kinematic conditions bring us to the domain of high-energy physics, meaning that the constituent masses of the bound system become increasingly less important. From the theoretical point of view, such a condition indicates an increased validity of the methods of high-energy physics (48) associated with the onset of light-front dynamics and calculational methods utilizing a new kind of (kinematic) small parameter, such as

$$\frac{q_-}{q_+} \sim \frac{p_{f-}}{p_{f+}} \ll 1, \quad 8.$$

where $q_\pm = q_0 \pm \mathbf{q}$ and $p_{f\pm} = E_f \pm p_f^z$ (the z axis is defined as the direction of $\mathbf{q}$). Such a small parameter permits a systematic accounting of the strong off-shell effects in the reaction mechanism of the external probe—bound nucleon scattering (49), as well as the possibility of self-consistent calculation of the final-state interaction of the fast struck nucleon with the correlated spectators within a generalized eikonal approximation (49–51).

The emergence of light-front dynamics in which the scattering process evolves along the light cone, $t \sim z$, is similar to that of deep-inelastic scattering (DIS) from a nucleon, in which the parton distribution of nucleons is probed. Light-front dynamics in DIS is the most natural approach given that, due to the light masses of quarks, one is dealing with a large contribution from vacuum fluctuations, which can be suppressed in the light-front or infinite-momentum reference frame (e.g., 48, 52).

Vacuum fluctuations also arise in relation to the high-momentum component of the nuclear wave function. When the momentum of the nucleon, p_i, becomes comparable to nucleon masses ($p_i \sim m_N$), the vacuum diagrams representing $N\bar{N}$ fluctuations become as important as the diagrams representing the "valence" component of the nuclear wave function (e.g., 46, 53). This

is an important problem that should be addressed by any theoretical study aiming to explore the high-momentum component of the nuclear wave function.

Another implication of light-front dynamics involves the emergence of the light-cone variables (α_i, p_T) that describe different nuclear "observables"[1] such as the nuclear spectral or light-front density functions. The variable α_i is analogous to the variable x of QCD and represents the light-cone nuclear momentum fraction carried by the constituent nucleon. It is defined as

$$\alpha_i = \frac{p_{i-}}{p_{A-}/A}, \qquad 9.$$

where p_{i-} and p_{A-} are "longitudinal" components of the light-cone momenta of the bound nucleon and nucleus.[2]

One of the advantages of (α_i, p_T) variables is their invariance with respect to Lorentz boosts in the **q** direction. Such a feature allows one to formulate nuclear spectral and density functions in a boost-invariant form. These functions are nucleonic analogs of unintegrated partonic distribution functions in QCD and can be systematically extracted from the analysis of nuclear processes. However, the extraction is possible only if the factorization between the reaction mechanism and nuclear light-front momentum distributions, as well as closure approximation for the final-state interaction contribution, is valid. All of these factors are analogous to DIS processes and can be systematically taken into account in the orders of the small parameter presented in Equation 8 (e.g., 49).

If the light-front spectral or density functions are extracted, they will represent a testing ground for the light-front nuclear wave function, $\psi_A(\alpha_1, p_{T1}, \alpha_2, p_{T2}, \cdots \alpha_A, p_{TA})$, through which the nuclear spectral and density functions are constructed as follows:

$$P_A^N(\alpha_i, p_{Ti}, \tilde{M}_N^2) = \sum_{j=1}^{A} \int \mid \psi_A(\alpha_1, p_{T1}, \alpha_2, p_{T2}, \cdots \alpha_A, p_{TA}) \mid^2 \delta(\alpha_i - \alpha_j)\delta^2(p_{Ti} - p_{Tj})$$
$$\times \delta(\tilde{M}_N^2 - \left(p_A - \sum_{j\neq i=1}^{A} p_j\right)^2 \prod_j^A \frac{d\alpha_j}{\alpha} d^2 p_{T_j} \qquad 10.$$

and

$$\rho_A^N(\alpha, p_T) = \int P_A^N(\alpha_i, p_{Ti}, \tilde{M}_N^2) \frac{1}{2} d\tilde{M}_N^2, \qquad 11.$$

normalized to the baryonic number of the nucleus,

$$\sum_N^A \int \rho_A^N(\alpha, p_T) \frac{d\alpha}{\alpha} d^2 p_T = A. \qquad 12.$$

Note that ρ_A^N can be related to $f_A(\alpha, p_T)$, which is analogous to the unintegrated partonic distribution function in QCD via

$$f_A(\alpha, p_T) = \frac{\rho_A^N(\alpha, p_T)}{\alpha}. \qquad 13.$$

These functions, extracted from the high-momentum-transfer semi-inclusive and inclusive processes, can provide a testing ground for the SRC properties of the nuclear wave function.

[1] They are not direct observables but rather can be extracted from different scattering processes involving nuclear targets.

[2] Note that in our definitions the direction of the z axis is defined by the direction of the momentum transfer q, which is the opposite of what is frequently defined in the QCD analysis of the nucleon wave function (e.g., 52).

2.3. Nuclear Dynamics at Sub-Fermi Distances: Proton–Neutron Dominance

The emergence of *NN* correlations in short-range nuclear dynamics creates the possibility of observing a host of new phenomena related to the rich structure of *NN* interactions at short distances. One such effect arises from the interplay of the central and tensor parts of the *NN* potential, in which, due to the repulsive core, the central part of the potential changes its sign at ∼1 fm to become repulsive; no such transition exists for the tensor part of the potential. As a result, at *NN* separations of $r_{NN} \sim 1 \pm 0.2$ fm, the tensor part of the *NN* interaction clearly dominates in comparison to the central potential.

This situation creates an interesting selection rule for the isospin composition of the SRCs. The tensor operator does not couple to isotriplet states—that is, $\hat{S}_{NN} \mid NN^{I=1}\rangle = 0$. The result is a situation in which the *NN* SRC is dominated by the isosinglet component of the *pn* pair. Note that here one considers the tensor interaction at distances of ∼1.2 fm, which cannot be reproduced on the basis of the pion exchange interaction alone. In phenomenological *NN* potentials, this part of the tensor interaction is parameterized to fit the *NN* phase shifts, and its origin is poorly understood.

If the contributions of *pp*, *nn*, and isotriplet *pn* SRCs are negligible, one would expect that in the momentum region of $\sim k_F$–600 MeV/*c* the momentum distribution in the *NN* SRC would be defined by the isosinglet *pn* correlation only. Using this fact and the local nature of SRCs, one predicts

$$n_{NN}(p) \approx n_{pn}(p) \approx n_d(p), \qquad 14.$$

for Equation 5, where $n_d(p)$ is the deuteron momentum distribution at $\sim k_F < p \leq 600$ MeV/*c*.

2.3.1. Two new properties of the high-momentum component of the nuclear wave function. We introduce the individual momentum distributions of the proton $[n_p^A(p)]$ and the neutron $[n_n^A(p)]$ such that

$$n^A(p) = \frac{Z}{A} n_p^A(p) + \frac{A-Z}{A} n_n^A(p), \qquad 15.$$

and $\int n_{p/n}^A(p) d^3p = 1$. Here, the terms in the sum represent the probability density of finding a proton or a neutron with momentum p in the nucleus.

2.3.1.1. Approximate scaling relation. By integrating Equation 15 within the momentum range of $\sim k_F$–600 MeV/*c*, one observes that the terms in the sum provide the total probabilities of finding a proton and a neutron in the *NN* SRC. Because the SRCs within the approximation in which the contributions from the isotriplet *NN* components are negligible consist only of isosinglet *pn* pairs, the total probabilities of finding a proton and a neutron in the SRC are equal. If one neglects the other possibilities for the SRC composition, one predicts that, in the $\sim k_F$–600 MeV/*c* region,

$$x_p \cdot n_p^A(p) \approx x_n \cdot n_n^A(p), \qquad 16.$$

where $x_p = Z/A$ and $x_n = (A-Z)/A$. This represents the first property, according to which the momentum distributions of the proton and the neutron, weighted by their respective fractions, are approximately equal.

The validity of the above approximate scaling rule is presented in **Figure 1**, which checks Equation 16 for the ^{3}He nucleus using the solution of Faddeev's equation (54) and for the ^{10}Be nucleus using the results of the VMC calculations in Reference 33. The figure shows that for ^{3}He, the proton momentum distribution dominates the neutron momentum distribution at low momenta simply because there are twice as many protons as neutrons in ^{3}He and no specific selection rules exist for the mean-field momentum distributions. The same is true for ^{10}Be, for

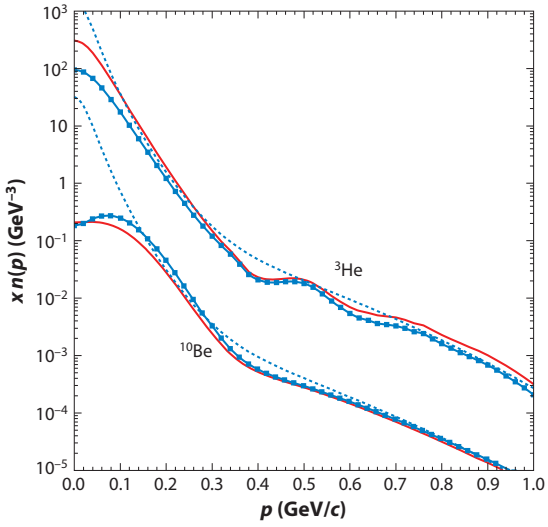

Figure 1

The momentum distributions of protons and neutrons, weighted by x_p and x_n, respectively. The dotted lines represent the prediction for the momentum distribution according to Equation 17. Modified from Reference 31.

which the neutron momentum distribution dominates at low momenta. However, for both nuclei, at ∼300 MeV/c the proton and neutron momentum distributions become close to each other up to the internal momenta of 600 MeV/c. This is the region dominated by tensor interaction. Note that similar features pertaining to all other asymmetric nuclei were calculated within the VMC method (33) for up to $A \leq 11$.

2.3.1.2. Fractional dependence of high-momentum components. Using Equations 5 and 14 for the high-momentum distribution $n^A(p)$ and using Equation 16 from Equation 15, one finds that, in the ∼k_F–600 MeV/c range,

$$n^A_{p/n}(p) \approx \frac{1}{2x_{p/n}} a_2(A,y) \cdot n_d(p), \qquad 17.$$

where $a_{NN}(A) \approx a_{pn}(A,y) \equiv a_2(A,y)$ and the nuclear asymmetry parameter is defined as $y = |x_n - x_p|$. For the situation in which the asymmetry parameter can be considered small ($y < 1$), the NN correlation factor is $a_2(A,y) \approx a_2(A,0)$ (31), which is a slowly changing function of nuclear mass for $A > 4$. We can now formulate the second property of the high-momentum distribution of nucleons: According to Equation 17, the probability of a proton or a neutron being in a high-momentum NN correlation is inversely proportional to its relative fraction (x_p or x_n) in the nucleus.

We can check the validity of this relation by comparing the momentum distribution in the NN SRC domain based on Equation 17 with the realistic distributions presented in **Figure 1**. To do so, we use the estimates of a_2 for ^{3}He and ^{10}Be (20, 32) and the deuteron momentum distribution, n_d, calculated using the Argonne V18 NN potential (55) that was also used to calculate the realistic momentum distributions for ^{3}He and ^{10}Be. These comparisons show that Equation 17 works rather well starting at 200 MeV/c and, surprisingly, up to the momenta ∼1 GeV/c, indicating that the 3N SRCs are parametrically small for all momenta (as discussed in Section 2.1).

2.3.1.3. Momentum sharing in asymmetric nuclei. The important implication of the second property of the high-momentum component of the nuclear wave function is that the relative

Table 1 Fractions of high-momentum protons and neutrons in nuclei A

A	P_p (%)	P_n (%)	A	P_p (%)	P_n (%)
12	20	20	56	27	23
27	24	22	197	31	20

number of high-momentum protons and neutrons becomes increasingly unbalanced with an increase in the nuclear asymmetry, y. To quantify this prediction, one uses Equation 17 to calculate the fraction of the nucleons having momenta $\geq k_F$ as

$$P_{p/n}(A,y) \approx \frac{1}{2x_{p/n}} a_2(A,y) \int_{k_F}^{\infty} n_d(p) d^3p, \qquad 18.$$

where we extend the upper limit of integration to infinity because of the smaller overall contribution from the $\geq$600 MeV/c region. **Table 1** presents the results of the calculation of $P_{p/n}$ values for medium to heavy nuclei, using the estimates of $a_2(A,y)$ from References 13, 18–20, and 32 and k_F from Reference 56.

The estimates in **Table 1** indicate that with the increase of asymmetry y, the imbalance between the high-momentum fractions of protons and neutrons grows. For gold, the fraction of high-momentum protons exceeds that of neutrons by as much as 50%.

Another implication of Equation 18 is that, due to the larger relative fraction of high momentum, the minority component should be more energetic in asymmetric nuclei than the majority component. Specifically, one expects a more energetic neutron than proton in ^{3}He, and the opposite for neutron-rich nuclei. This expectation is confirmed by ab initio calculations of $p-$ and $n-$ kinetic energies for all nuclei (currently up to $A \leq 11$) (**Table 2**) (31).

2.4. Three-Nucleon Correlations

Above, we define a nucleon to be in a NN SRC if its momentum exceeds k_F and is almost entirely compensated for by the momentum of the correlated nucleon in the nucleus. For a nucleon to be in a 3N SRC, we assume, again, that its momentum must significantly exceed k_F but, in this case, is balanced by two correlated nucleons with momenta $>k_F$. In both cases, the center-of-mass momentum of the SRC, p_{cm}, is less than or equal to k_F.

Table 2 Kinetic energies (E_{kin}, in MeV) of protons and neutrons across several nuclei

A	y	E^p_{kin}	E^n_{kin}	$E^p_{kin} - E^n_{kin}$
^{8}He	0.50	30.13	18.60	11.53
^{6}He	0.33	27.66	19.06	8.60
^{9}Li	0.33	31.39	24.91	6.48
^{3}He	0.33	14.71	19.35	−4.64
^{3}H	0.33	19.61	14.96	4.65
^{8}Li	0.25	28.95	23.98	4.97
^{10}Be	0.20	30.20	25.95	4.25
^{7}Li	0.14	26.88	24.54	2.34
^{9}Be	0.11	29.82	27.09	2.73
^{11}B	0.09	33.40	31.75	1.65

In principle, the complete nuclear wave function should contain the above-described property of *NN* and 3*N* SRCs. Unfortunately, calculating such wave functions from first principles is currently impossible because of the poorly understood strong interaction dynamics at short nuclear distances, as well as relativistic effects that become increasingly important at high momenta of nucleons involved in SRCs. However, recent theoretical studies have provided a sufficient roadmap for meaningful experimental exploration of 3*N* SRCs.

One result of such studies is that the irreducible 3*N* forces contribute to 3*N* SRCs only at very large nuclear excitation energies of $>2(\sqrt{p^2+m_N^2}-m_N)$ (where $p \gtrsim 700$ MeV/c), and are otherwise negligible (29). Thus, outside of such kinematic regions, the dynamics of 3*N* SRCs are defined by two sequential short-range *NN* interactions (57). Such a situation highlights the difficulties of experimentally identifying 3*N* SRCs. With regard to extracting the nuclear spectral function, the separation of 3*N* SRCs is problematic because the expected enhancement in recoil energy distribution at $E_{\rm rec} \approx p^2/4m_N$ is very broad without a discernible maximum (29). With regard to the momentum distribution, because the 3*N* SRCs are subleading compared with *NN* SRCs (58; see also Section 2.1), they are parametrically small for all values of p, making the momentum distribution $n_A(p)$ rather insensitive to 3*N* SRCs.

Thus, one of the problems in the experimental identification of 3*N* SRCs is the proper identification of the variables that can unambiguously discriminate 3*N* and *NN* SRCs. To this end, the relevant variable is the light-cone momentum fraction, α_i, defined in Equation 9. Due to the short-range nature of the nuclear forces, the condition

$$j-1 < \alpha_i < j \qquad 19.$$

will ensure that scattering from $(j \times N)$ SRCs is being probed (46, 58). Thus, one expects that the extraction of $\rho_A(\alpha_i)$ at $\alpha_i > 2$ will ensure the dominance of 3*N* SRCs.

2.4.1. Dynamics of three-nucleon short-range correlations. In light of the recent observation of the strong dominance of *pn* pairs in *NN* SRCs (see Section 2.3) for momenta of 250–600 MeV/c, as well as the expectation (discussed above) that 3*N* SRCs are predominantly due to two successive *NN* short-range interactions, one predicts that *pn* dominance would be strongly implicated in 3*N* SRCs as well. This means that 3*N* SRCs should have a predominantly *ppn* or *nnp* composition and that *ppp* and *nnn* configurations should be strongly suppressed. **Figure 2*a*** depicts a diagram representing the light-cone density matrix of 3*N* SRCs; the three nucleons are in either a *ppn* or an *nnp* configuration. The light-front spectral function according to **Figure 2*a***, calculated within the effective Feynman diagrammatic approach (57, 59), is expressed through the light-front density functions of *NN* SRCs as follows:

$$P^N_{A,3N}(\alpha_1, p_{1,\perp}, \tilde{M}_N) = \int \frac{3-\alpha_3}{2(2-\alpha_3)^2}\rho_{NN}(\beta_3, p_{3\perp})\rho_{NN}(\beta_1, \tilde{k}_{1\perp})2\delta(\alpha_1+\alpha_2+\alpha_3-3)$$
$$\delta^2(p_{1\perp}+p_{2\perp}+p_{3\perp})\delta(\tilde{M}_N^2 - M_N^{3N,2})d\alpha_2 d^2p_{2\perp}d\alpha_3 d^2p_{3\perp}, \qquad 20.$$

where, within the colinear approximation, $\beta_3=\alpha_3$, $\beta_1=2\alpha_2/(3-\alpha_3)$, and $\tilde{k}_{1\perp}=p_{1\perp}+(\beta_1/2)p_{3\perp}$ (α_i represents the light-cone momentum fraction of the 3*N* SRCs carried by the correlated nucleon i). The 3*N* SRC spectral function uses as an input the density functions of *NN* SRCs, ρ_{NN}, which can be extracted from studies of *NN* correlations.

The dynamics of 3*N* SRCs, according to the correlation scenario of **Figure 2*a***, have several unique features that can be verified experimentally. One is that the per nucleon probability of finding a nucleon in a 3*N* SRC, a_{3N}, should be proportional to the square of the probability of

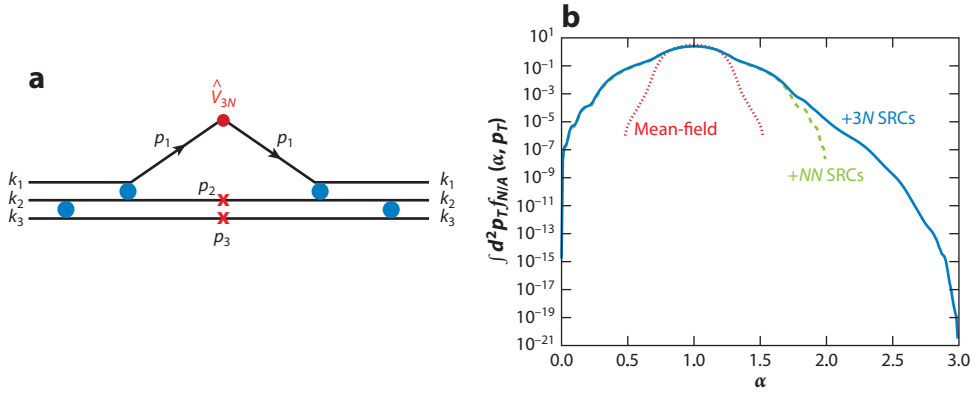

Figure 2

(*a*) 3*N* short-range correlations (SRCs) due to sequential *NN* SRCs. (*b*) The α distribution of the light-front density matrix. The dotted line represents the nuclear mean-field contribution only. The dashed green line represents the mean-field and *NN* SRC contributions. The solid blue line represents the mean-field, *NN*, and 3*N* SRCs. Panel *a* modified from Reference 57. Panel *b* modified from Reference 59.

finding a nucleon in a *NN* SRC, a_{NN}. Specifically,

$$a_{3N} \sim a_{NN}^2. \qquad 21.$$

Another feature is that the dominant 3*N* SRC configuration will be one in which the *NN* spectator system has a minimal mass $m_S \gtrsim 2m_N$, corresponding to low relative momentum in the recoil *NN* system, $k_{NN} = (\sqrt{m_S^2 - 4m_N^2})/2$. The condition $k_{NN} \ll m_N$, and the fact that isotriplet *NN* states with low relative momenta are strongly suppressed (60) compared with the isosinglet states, results in a strong dependence of the 3*N* SRCs on the isospin structure of the *NN* recoil system. Specifically, 3*N* SRCs are dominated by configurations in which the recoil *NN* system is in the isosinglet state.

We conclude our discussion of 3*N* SRCs by illustrating a calculation of the p_T -integrated light-front density function (59) in **Figure 2*b***, which depicts mean-field, *NN*, and 3*N* SRC contributions. The figure shows that, despite the fact that the 3*N* SRCs are subleading to the *NN* SRCs, they are well separated in α, as discussed above.

2.4.2. Nonnucleonic degrees of freedom and medium modifications. Recent experimental and theoretical studies of SRCs have advanced our understanding of the domain of *NN* correlations for momenta up to 600 MeV/*c*, providing an important foundation for the extension of SRC studies to the uncharted territory of hadron–quark transitions. Studies of the isospin structure of *NN* SRCs (21–23) not only found *pn* dominance but also observed that the sum of the absolute *pp* and *pn* probabilities is close to unity, indicating that practically all nucleons in this momentum range (with an accuracy on the order of a few percent) belong to *NN* SRCs. This is an important observation because it excludes, at a high level of confidence, the explicit nonnucleonic degrees of freedom in this momentum range.

By contrast, nucleons are composite particles, so internucleon interactions in SRCs should lead to a deformation of the bound nucleon wave function. Such a modification of the bound nucleon is manifested in the experimental observation of the difference between partonic distributions of free and bound nucleons, commonly referred to as the EMC effect (61). The most recent EMC effect measurement was performed for a wide range of nuclear targets, focusing on light nuclei (26); it

yielded an interesting observation that the extent of the modification is proportional not to the average density of nuclei but rather to the local density at which the bound nucleon is probed. This observation may indicate an important role that SRCs play in the medium modification of the partonic distribution of nucleons in the nuclei. This expectation is enhanced by the observation of an apparent correlation between the strengths of the EMC effect and *NN* SRCs (27, 28). Similar apparent correlations (28) have also been observed between EMC effects and nuclear excitation energies, indicating the enhanced role of SRCs in the modification of the internal structure of bound nucleons.

2.5. Nuclear Dynamics at Core Distances

One of the most fascinating aspects of nuclear physics at short distances is the repulsive core. With the continued advances in high-energy and high-intensity accelerators such as CEBAF12, LHC, and J-PARC, as well as the proposed Electron–Ion Collider (EIC), the systematic exploration of nuclear dynamics at core distances has become a real possibility. We characterize core distances as those where the probed relative distance is smaller than the radius of the nucleon, which means substantial overlap between two nucleons in the nuclear medium.

Currently, very little is known about the structure and the dynamics of nuclear repulsion at core distances. Modern *NN* potentials employ the Woods–Saxon ansatz, whereas models based on one-boson exchanges introduce vector meson exchanges to reproduce repulsion at distances smaller than the size of the exchanged mesons. QCD-based models employ other extreme scenarios in which two nucleons are collapsed into a six-quark state.

The relative momenta in the *NN* system that will be sensitive to the core dynamics can be estimated on the basis of the threshold of the inelastic $N \rightarrow \Delta$ transition,

$$\sqrt{M_N^2 + p^2} - M_N \geq M_\Delta - M_N, \qquad 22.$$

which results in $p \geq 800$ MeV/c. Thus, one of the direct ways of reaching the core is to probe internal momenta in the ∼1 GeV/c region.

Experimentally, it is possible to probe internal momenta in nuclei in the range of ≥1 GeV/c by considering DIS from superfast quarks in nuclei (25, 62). We define superfast quarks as partons that have been probed via nuclear DIS scattering at $x > 1$. Because partons cannot carry momentum fractions larger than one in an isolated nucleon at rest, DIS scattering at $x > 1$ is possible if partons in nearby nucleons are sharing momentum. This requires the two nucleons to be in very close proximity.

Superfast quarks can probe high-density fluctuations in the nuclear medium for two basic reasons. The first is kinematical. The initial longitudinal momentum of a nucleon probed in DIS scattering is (62)

$$p_i^z = m\left(1 - x - x\left[\frac{W^2 - m^2}{Q^2}\right]\right), \qquad 23.$$

where W is the final mass produced on the nucleon in the nucleus. In the DIS region at $W \geq 2.5$ GeV, the virtual photon will probe a nucleon with momentum $p_i^z \sim -1$ GeV/c (**Figure 3*a***).

The second reason that superfast quarks can probe high-density fluctuations in the nuclear medium is dynamic. Due to QCD evolution, the parton at x is evolved from the original partons with momentum fraction $x_0 \geq x$, which increases with Q^2. Thus, the alternative way of probing short space-time separations in the nuclear medium would be a measurement with fixed x and increasingly large Q^2. Such studies will probe QCD dynamics in extreme nuclear conditions with the potential of opening up uncharted territory for QCD exploration in the nuclear medium.

The extreme nuclear dynamics may include multinucleon SRCs (25, 59, 62); explicit quark degrees of freedom, such as six-quark clusters (63); or single quark momentum exchanges between

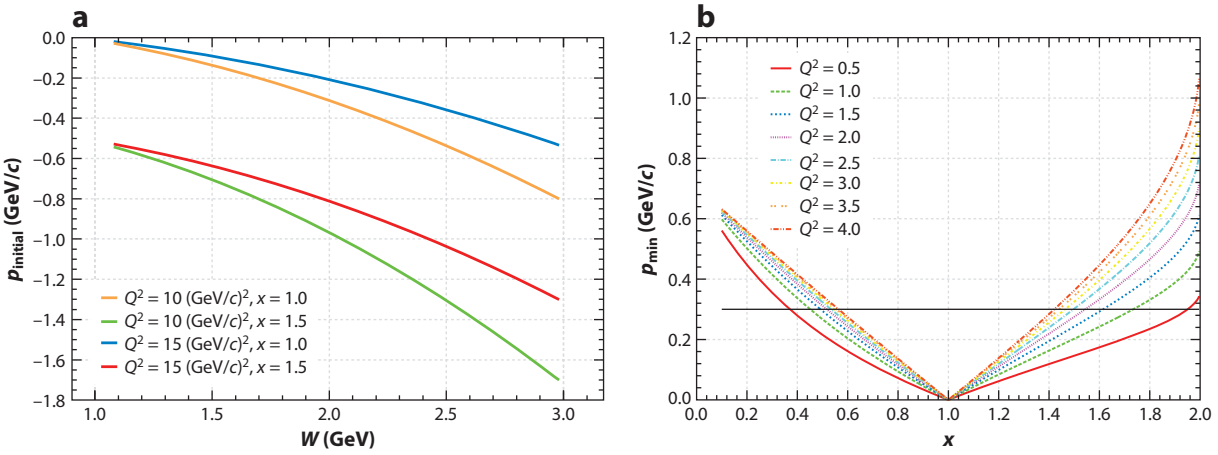

Figure 3

(*a*) Dependence of $p_{\rm in}^z$ on the final mass W produced in deep-inelastic scattering off the bound nucleon in the nucleus. (*b*) The minimum momentum for quasi-elastic $\gamma^* + NN \rightarrow N + N$ scattering as a function of x for different values of Q^2.

strongly correlated nucleons (64). Superfast quarks can be probed in different processes, including inclusive DIS from nuclei at $x > 1$ (25, 62, 64), semi-inclusive nuclear DIS with tagged spectator nucleons (65, 66), DIS production in the forward direction with $x_{\rm F} > 1$, or large transverse momentum dijet production in $p + A \rightarrow$ dijet $+ X$ reactions at LHC kinematics (59).

3. RECENT ADVANCES IN EXPERIMENT

The beginning of JLab's operation in the 1990s represented a new era of exploration of the nuclear structure at short distances. The SRC program included high-Q^2 ($\geq$1 GeV^2) inclusive $A(e, e')X$ measurements (18–20, 67–69) complemented with semi-inclusive triple coincidence (22–24, 70) and exclusive deuteron electrodisintegration (35, 71) experiments. In the following subsections, we review the most important recent results for *NN* SRCs from inclusive and triple coincidence measurements.

3.1. Inclusive High-Q^2 Processes at $x > 1$

The main motivation of any experiment studying SRCs is to probe the bound nucleon with a momentum exceeding the characteristic Fermi momentum: $k_{\rm F} \sim 250$ MeV/c. As discussed in Section 2.2, the most relevant quantity for this purpose is the light-front momentum fraction, α_i (Equation 9), for which choosing the condition of Equation 19 will enable one to probe j-nucleon SRCs. The technical question for any given experiment is how to determine the parameter α_i for different regions of nucleonic SRCs.

One way to achieve such a measurement is in quasi-elastic nuclear reactions in which, from the condition $(p_i + q)^2 = M_N^2$, one obtains

$$\alpha_i = x\left(1 + \frac{2\,p_{i,z}}{q_0 + |q|}\right) + \frac{M_N^2 - m_i^2}{2m_N q_0}, \qquad 24.$$

where $p_{i,z}$ is the longitudinal momentum of the initial nucleon along the direction of the transferred momentum q in the nuclear rest frame. This equation shows that in the asymptotic limit of large

Q^2, $\alpha_i \approx x$; therefore, choosing $x > 1$ allows one to satisfy the necessary conditions to probe multinucleon correlations. Because x is defined by the kinematics of electron scattering only, $x = Q^2/(2M_N q_0)$, this consideration indicates that *NN* correlations can be probed in inclusive $A(e,e')X$ experiments.

3.1.1. Probing two-nucleon short-range correlations in the $1 < x < 2$ region. The above discussion considers asymptotically large Q^2 to illustrate the simple relation between α_i and x. At finite values of Q^2 one can use Equation 24 to identify the optimal kinematics for the separation of *NN* correlations. Note that Equation 24 can be solved for the longitudinal component of p_i, which represents the minimal magnitude of the momentum of the bound nucleon. One can then find the suitable x, Q^2 kinematics for which $|p_{\min}| > k_F$ in order to isolate *NN* SRCs. **Figure 3*b*** shows the relationship between $p_{\min}$, x, and Q^2, implying that, in order to observe *NN* SRCs at $x \geq 1.4$, a Q^2 value of 1.4 GeV^2 is required. The figure also shows that one cannot probe correlations at $Q^2 \leq 1$ GeV^2. The existence of such a threshold in Q^2 was experimentally observed in the dedicated measurement of inclusive cross sections at $x > 1$ (18).

The minimum initial momentum of the bound nucleon can be used to estimate (13) the corresponding light-cone momentum fraction α_{NN}, which is defined by the parameters of the scattered electron only:

$$\alpha_{NN} = 2 - \frac{q_- + 2m_N}{2m_N}\left(1 + \frac{\sqrt{W^2 - m_N^2}}{W^2}\right). \qquad 25.$$

Here, $W^2 = 4m_N^2 + 4m_N\nu - Q^2$. The advantage of discussing the inclusive cross section based on the α_{NN} representation is that in the high-energy limit one expects the inclusive cross section to factorize into the product of the cross section of electron-bound nucleon scattering and the light-front density matrix of the nucleus, $\rho_A(\alpha_{NN})$. Therefore, in principle, inclusive scattering enables the extraction of $\rho_A(\alpha_{NN})$ from the measured cross sections.

The first indication of the onset of the *NN* SRC regime in inclusive scattering is the appearance of the plateau in the ratios of the cross sections measured for nuclei A to the deuteron (20) or ^{3}He (18, 19) in the $x > 1$ region at large Q^2. This plateau is the result of the nuclear high momentum's factorization in the form of Equation 17. **Figure 4*a*** presents recent results of such measurements for ^{3}He/D (deuterium) and ^{12}C/D ratios.

One of the interesting features of the x dependence of the experimental ratios is that the threshold for the onset of the scaling is extended further in x for ^{12}C compared with ^{3}He. This feature can be understood from the fact that, for heavier nuclei, k_F is higher and the *NN* SRC region begins at higher x values, as the mean-field contribution persists longer.

Another feature observed in the x dependence is that for a given nucleus the onset of scaling is Q^2 dependent. Such Q^2 dependence is more visible in the ^{12}C/D ratios, where one observes that the data at higher Q^2 values rise toward the plateau value sooner. Such Q^2 dependence can be understood from Equation 25, where for a given x value the α_{NN} values change with Q^2. However, if we consider the α_{NN} distribution of the ratios instead of x, then such a Q^2 dependence should diminish. This is indeed what has been observed experimentally (**Figure 4*b***). This fact is one of the most important arguments for the validity of the *NN* SRC picture of inclusive scattering.

Even though the observation of the plateau is consistent with the expectation of scattering from *NN* SRCs, to study the dynamics of the SRCs in more detail, one needs to address several theoretical issues. One issue is the shape of the ratios. If the contribution to the $x > 1$ region is only from *NN* SRCs, then one expects the shape of the plateau to be the same for ^{3}He and ^{12}C and for other nuclear targets (20). The nuclear cross sections can extend up to $x \approx A$, meaning that the

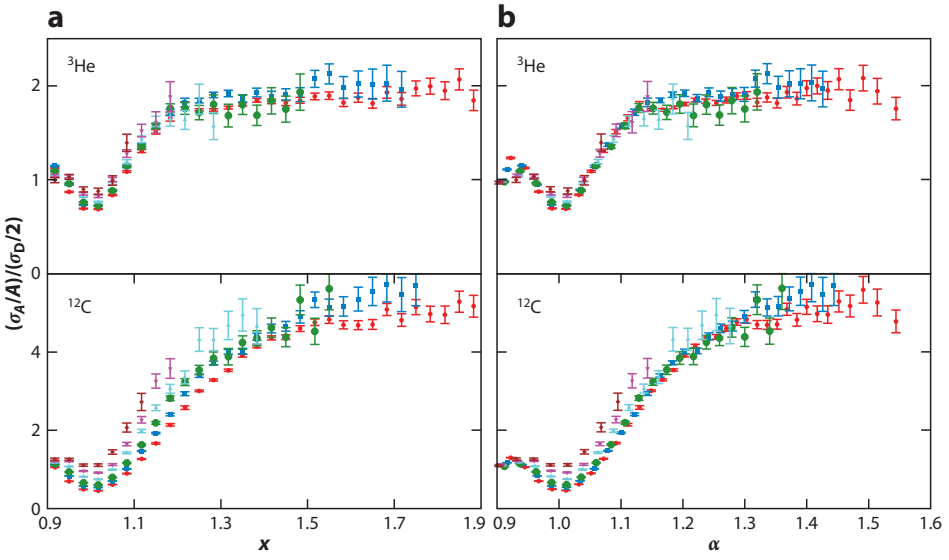

Figure 4

σ_A/σ_D versus (*a*) x and (*b*) α for selected targets from the JLab E02-019 experiment. The different sets of colored points correspond to data taken at different Q^2 values, ranging from 2.5 GeV^2 to 7.4 GeV^2 (as evaluated at $x = 1$). Only points with uncertainties below 10% are shown, meaning that only the lowest Q^2 data reach the highest x values.

D cross section has to go to zero by $x = 2$, whereas for $A > 2$, strength continues well past that. Therefore, we expect a slight rise in the A/D ratios as we approach the $x = 2$ limit. This increase, due to different rates of cross-section fall-off between A and D, becomes larger with increasing nucleus size. Additionally, for $A > 2$, the correlated pair will experience center-of-mass motion in the field of the other nucleons, which will distort the momentum distribution compared with that of the deuteron, enhancing the high-momentum tail region. Finally, $A > 2$ nuclei will have contributions from 3*N* correlations that could be appearing near the $x \approx 2$ region.

All of the above factors are essential for the extraction of the parameter $a_2(A, z)$ from the cross-section ratio. A correction is required for the center-of-mass motion of the pair, and a cut in α must be placed to isolate the region that is dominated by *NN* correlations. The most recent analysis (20) did both, with a cut of $1.5 < \alpha < 1.9$ and rudimentary center-of-mass motion calculations, yielding corrections up to 20% for heavy nuclei. The calculation entails comparing a calculated deuteron momentum distribution with one smeared with realistic center-of-mass motion (72). Better evaluations of the center-of-mass corrections are desirable for future experiments.

3.1.2. Probing three-nucleon short-range correlations in the $x > 2$ region. According to Equation 19, accessing the region of $\alpha_i \geq 2$ will allow us to probe 3*N* SRCs. However, whereas in the case of *NN* SRCs one needs to simply go beyond k_F, for 3*N* SRCs the transition from *NN* to 3*N* SRCs is more complicated. Early measurements of inclusive cross-section ratios at $x > 1$ relied on the idea that a second plateau corresponding to 3*N* strength should be observed at $2.4 \lesssim x \lesssim 3$ and $Q^2 \geq 1.4$ GeV^2, analogous to the *NN* SRC plateau in the $1.5 \lesssim x \lesssim 1.9$ region. Data from JLab's Hall B that appeared to support this observation were first published (19) with ^{4}He/^{3}He, ^{12}C/^{3}He, and ^{56}Fe/^{3}He ratios. However, a later experiment in JLab's Hall C (20) did not observe a second plateau, although the uncertainties were significantly higher, so the possibility

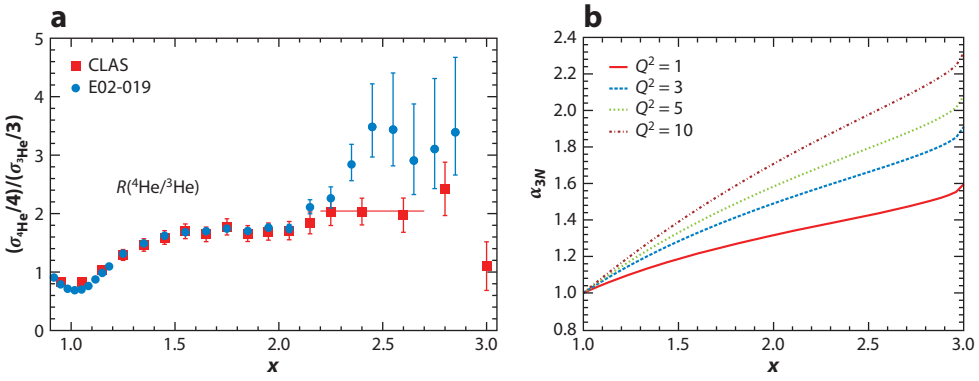

Figure 5

(*a*) The ratio of the (e, e') cross sections of ^{4}He and ^{3}He targets as a function of x. (*b*) The α_{3N} relation to x for different values of Q^2. Panel *a* modified from Reference 20.

could not be excluded. The two sets of data showed excellent agreement in the *NN* correlation region (**Figure 5**). One possible explanation for this discrepancy was the different kinematics of the two measurements. Because a kinematic threshold exists for the observation of *NN* correlation plateaus, a 3*N* analog is expected, but the Q^2 threshold is not as easily obtained. The CEBAF Large Acceptance Spectrometer (CLAS) data were taken at an average Q^2 value of 1.4 GeV^2 compared with 2.7 GeV^2 for the Hall C data. Because 1.4 GeV^2 is the threshold for *NN* correlations, one would expect that a higher value would be needed in order to observe a 3*N* plateau, suggesting that the Q^2 value of the CLAS data may have been too low. However, this does not explain the apparent plateau at $x > 2.25$.

A recent reanalysis of the CLAS data (73) shows that this plateau could be the effect of bin migration. Both experiments measured cross sections as a function of the scattered energy of the electron (E') and converted them to x. The resolution of the CLAS spectrometer is almost an order of magnitude lower than that of the high-momentum spectrometer in Hall C, and at large x values ($x \geq 2$), it is larger than the size of the bins. This effect, combined with the fact that the ^{3}He cross section exponentially approaches zero in this region, results in significant bin migration. Specifically, most of the points making up the 3*N* SRC plateau in the CLAS data (19) came from the same E' bin.

The question remains concerning why JLab experiment E02-019, whose data were taken at higher values of Q^2 with a high-resolution spectrometer, did not observe a 3*N* SRC plateau. Consider the variable α_{3N}, a counterpart of α_{NN} for *NN* SRCs in Equation 25. Here, α_{3N} properly accounts for the mass of the 3*N* system and the recoil of the *NN* system (assuming a configuration in which one high-momentum nucleon is balanced by two others). Theoretical analyses of the hadroproduction reaction suggest that a minimum α value of 1.6 is required to isolate high-momentum nucleons born in 3*N* SRCs. **Figure 5*b*** shows that a minimum Q^2 value of 5 GeV^2 is needed in order to access this region, whereas the existing JLab data were taken below 3 GeV^2. However, Q^2 values at or above 5 GeV^2 are within reach at JLab with the 12-GeV upgrade. Moreover, future analyses should be performed using the $\alpha_{NN,3N}$ variables, rather than the traditional x, as they can unambiguously connect to the *NN* and 3*N* SRC dominance regions.

3.1.3. Upcoming inclusive measurements. JLab experiment E08-014 took data in Hall A with both of the high-resolution spectrometers, focusing on the $x > 2$ region with the goal of mapping

the onset of the 3*N* plateau via a Q^2 scan. The experiment also took data with ^{40}Ca and ^{48}Ca targets in order to study the isospin dependence of SRCs. **Figure 5*b*** suggests that the kinematics probed by this experiment at 6 GeV were not sufficient to observe a 3*N* plateau, but the precision of the data on the calcium target should be sufficient to yield interesting results.

JLab plans to perform additional inclusive SRC measurements for the 12-GeV era. These include high-precision measurements of $A = 3$ nuclei in Hall A that can be compared with calculations. Additionally, experiment E12-06-105 will take data on a variety of both light and heavy nuclei with Q^2 scans in order to explore the onset of the 3*N* plateau as well as to study the nuclear dependence of *NN* SRCs. The most important aspects of SRC exploration with 12-GeV energy are the possibility of unambiguous verification of the existence of 3*N* SRCs, access to the domain of the nuclear repulsive core in the *NN* correlation, and the ability to probe superfast quarks in deep-inelastic inclusive processes at $x > 1$ kinematics (see Section 4.2).

3.2. Nucleon–Nucleon Correlations and the EMC Effect

In 1983, the European Muon Collaboration (EMC) (61) published a surprising DIS result showing a dip in the per nucleon cross-section ratio of heavy to light nuclei when plotted versus x, a ratio that one would naïvely expect to be unity up to the Fermi motion effects. This result has been reproduced many times (26, 74–76), and the dip in the cross-section ratio is now commonly referred to as the EMC effect. Many possible explanations for this unexpected phenomenological result have been put forth over the years, but no definitive consensus regarding the EMC effect puzzle has been reached (77–80).

In 2011, Weinstein et al. (27) noted a linear relation between the magnitude of the EMC effect and the magnitude of the aforementioned inclusive high-momentum plateaus (**Figure 6**). There is a clear linear relationship between these two seemingly disconnected phenomena, which may be due to the short-range behaviors of the *pn* pairs in the nucleus (36). Later publications based on more data reported similar behaviors, although the data alone do not provide a clear reason for the relationship (28, 81).

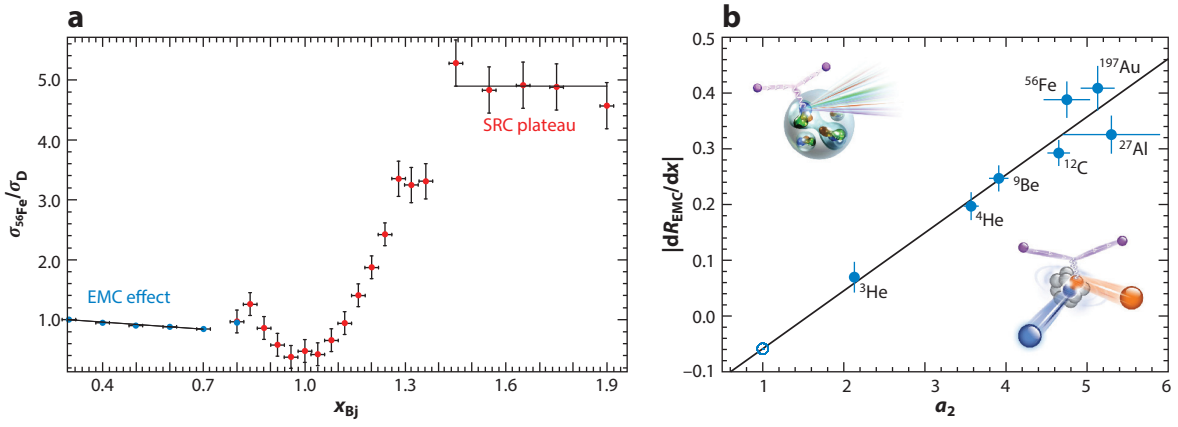

Figure 6

(*a*) The Bjorken x dependence of the ratio of the inclusive ($e e'$) cross section of ^{56}Fe to the deuteron targets. (*b*) The observed correlation between the strengths of the EMC effect and *NN* short-range correlations (SRCs). Panel *a* modified from Reference 79. Panel *b* modified from Reference 80 with permission from JLab.

A modern review on the topic of *NN* corrections and the EMC effect (36) points to the fact that the strongly interacting *pn* pairs, which are a universal aspect of high-momentum nucleons in the nucleus, may also be responsible for the modification of the structure functions. For a complete discussion of the possible connections between *NN* correlations and quarks, see the review by Hen et al. (36).

3.3. Recent $(e, e'p)$ Measurements

Although nuclear theory long ago identified the need to include the high-momentum component in nuclear momentum distributions, and all modern *NN* potentials generate a high-momentum tail in the nuclear wave function with a strength far beyond what one would expect from an independent particle model, it is nevertheless quite challenging to directly probe the high-momentum component of the nuclear wave function. The above-mentioned inclusive results, as well as elastic nuclear scattering at large momentum transfers, provide a very strong indication of initial-state SRCs in the nuclear wave function, allowing one to estimate their overall strength. However, these processes do not permit one to extract the shape of the high-momentum distribution; rather, they allow one to probe only the integrated characteristics of SRCs. Thus, a significant experimental effort was initiated to measure knockout $(e, e'p)$ reactions to determine the shapes of high-momentum distributions at large values of residual nuclear excitation energies.

Early nucleon knockout experiments, with $(e, e'p)$ missing momenta lower than the Fermi momentum, successfully extracted the momentum distribution of the nucleon in the nucleus from the measured cross sections (82). At that time, it was conjectured that by simply extending to a larger momentum transfer one could extract the high-momentum part of the momentum distribution; here, however, nature would not be so kind. As shown by many experiments, reaction mechanisms, final-state interactions, or virtual nucleon excitations can quickly dominate the high-momentum signal (83), making it extremely challenging to determine the initial-state high-momentum distribution.

Part of the problem was the limited kinematics reach of the accelerators at that time, which limited the high-missing-momentum data to the region between the quasi-elastic peak and the Δ resonance, commonly known as the dip region. Following the advent of JLab, the first $(e, e'p)$ experiments were measured at large missing momentum on the quasi-elastic peak ($x \approx 1$). The kinematics of these measurements corresponded to the large transverse component of the missing momentum, resulting in a strong dominance of final-state interactions in the measured cross sections (84–86).

Extending the kinematics to $Q^2 = 3.5$ GeV/c^2 and making use of the properties of high-energy small-angle rescatterings to minimize final-state interaction effects have enabled the high-momentum component of the deuteron to be isolated with minimum model dependence (35). Future $(e, e'p)$ experiments at JLab with a 12-GeV beam will extend these kinematics even further, to both large missing momentum, $Q^2 \gg 1$, and $x > 1$ (87). These kinematics will ideally satisfy the conditions of Equation 7, allowing access to the momentum distribution of the deuteron at unprecedentedly high values. Asymmetry measurements have also been useful in isolating SRC effects, although to date the unambiguous interpretation of the data has required the inclusion of several effects associated with long-range two-body currents (88–90).

3.4. Triple Coincidence Processes

One of the most important recent advances in studies of the structure of SRCs has been made in triple coincidence experiments (21–24). The possibility of reaching high-enough momentum

transfer that allows one to distinguish between a struck nucleon and the nucleon recoiled from the SRC enables one to obtain important information about the dynamics and composition of SRCs.

3.4.1. Angular correlation of nucleons in two-nucleon short-range correlations. The kinematics of these experiments were close to those in Equation 7, in which the detected recoil nucleon with momentum p_r can be associated with the spectator nucleon. From the theoretical point of view, such a reaction within the plane wave impulse approximation (PWIA) is described as follows:

$$\frac{d\sigma}{d\Omega_{e'} dE_{e'} d^3 p_N d d^3 p_r} = \frac{F_N}{F_A} \sigma_{eN} \cdot D_A(p_i, p_r, E_r), \qquad 26.$$

where the decay function $D_A(p_i, p_r, E_r)$ (25, 29, 58) describes the probability that, after a nucleon with momentum p_i is instantaneously removed from the nucleus, the residual $(A-1)$ nuclear system will have residual energy $E_R = q_0 - T_f$ and will contain a nucleon in the nuclear decay products with momentum p_r. Note that if factorization of the nucleon electromagnetic current is justified, then the decay function can be generalized within the distorted wave impulse approximation (DWIA), which will include effects due to final-state interactions between the outgoing nucleons and the residual nucleus. One advantage of the high-energy kinematics of Equation 7 is the emergence of the eikonal regime, in which case final-state interaction effects can be isolated to interfere only minimally with the SRC signatures (29, 60).

If a *NN* SRC is probed in the $A(e, e', N_f, N_r)X$ reaction, then the prominent signatures will be that the decay function will exhibit a strong correlation between $\mathbf{p_i} = \mathbf{p_f} - \mathbf{q}$ and $\mathbf{p_r}$, such that

$$\mathbf{p_i} \approx -\mathbf{p_r} \qquad 27.$$

if both $p_i > k_F$ and $p_f > k_F$. This relation indicates a strong angular correlation between the direction of the yield of recoil nucleons and the direction of the struck nucleon momentum in the initial state.

Such an angular correlation was observed for the first time in the high-momentum-transfer $p + {}^{12}\mathrm{C} \to p + p + n + X$ measurement by BNL's E850 experiment (91, 92). This experiment measured the recoil neutrons produced in coincidence with high-energy proton knockout and observed a strong back-to-back angular correlation between the direction of the measured recoil neutrons and the reconstructed momentum of the initial bound proton once these momenta exceeded k_F. Remarkably, no correlation was observed when the reconstructed momentum was lower than k_F.

The existence of such correlations between nucleons in the *NN* SRC was confirmed by a JLab Hall A experiment (22) that measured the ${}^{12}\mathrm{C}(e, e', p_f, N_r)$ reaction in which the struck proton p_f was measured in coincidence with either a recoil proton or a neutron, N_r. The kinematics of the experiment were set at $Q^2 \approx 2$ GeV^2 and $x \approx 1.2$, with missing momenta in the range 300–600 MeV/c. With the kinematic condition of Equation 7 satisfied, the experiment observed a clear signature of the correlation between the strength of the cross section and the relative angle (γ) of initial momentum $\mathbf{p_i}$ and recoil nucleon momentum $\mathbf{p_r}$.

Figure 7*a* shows the distribution of events in $\cos\gamma$ for the highest p_i setting of 550 MeV/c (22). The distribution strongly peaks near $\cos\gamma = -1$, corresponding to the back-to-back initial momenta of the struck and recoil protons. In the simulated distribution for scattering from a moving pair, the pair's center-of-mass momentum was taken to be a Gaussian distribution with a width of 0.136 GeV/c. This width is consistent with the one deduced from the (p, ppn) experiment at BNL (92), as well as with theoretical calculations (72). **Figure 7*a*** also depicts the angular correlation for the random background as defined by a time-window offset from the coincidence peak, which shows the effect of the acceptance of the spectator proton detector.

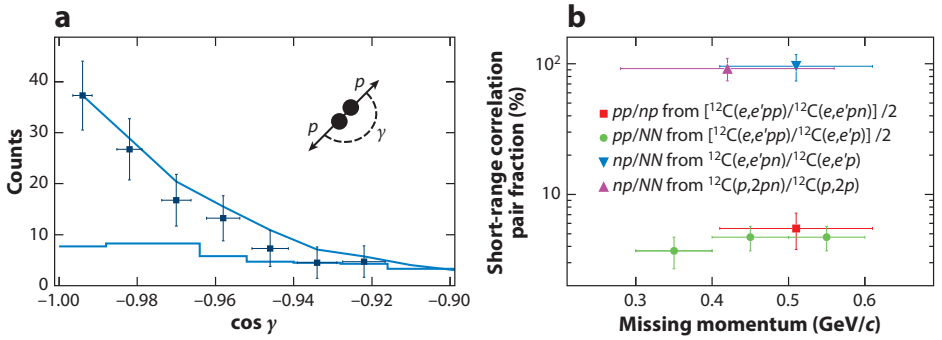

Figure 7

(*a*) The distribution of the cosine of the opening angle between $\mathbf{p_i}$ and $\mathbf{p_r}$ for $p_i = 0.55$ GeV/c for the $^{12}\mathrm{C}(e, e'pp)$ reaction. The solid curve represents the simulated distribution for scattering from a moving pair. (*b*) The fraction of correlated pair combinations in carbon as obtained from the $A(e, e'pp)$ and $A(e, e'pn)$ reactions (23), as well as from previous $(p, 2pn)$ data (21). Panel *a* modified from Reference 22. Panel *b* modified from Reference 23.

3.5. Observation of Proton–Neutron Dominance in ^{12}C

In addition to the observation of a strong angular correlation between the recoil neutron and struck proton momenta emerging from *NN* SRCs, the $p + {}^{12}\mathrm{C} \rightarrow p + p + n + X$ experiment (92) determined that $(49 \pm 13)\%$ of the events with fast initial protons have correlated backward-going fast recoil neutrons. A theoretical analysis of this experiment (21), based on modeling of the nuclear decay function of Equation 26 (93), enables the above-mentioned event rate to be related to the quantity $P_{pn/pX}$, a quantity that represents the probability of finding a *pn* correlation in the pX configuration, which contains at least one proton with $p_i > k_\mathrm{F}$, yielding

$$P_{pn/pX} = 0.92^{+0.28}_{-0.18}. \qquad 28.$$

This result indicates that, approximately 92% of the time, the removal of a proton from the nucleus with initial momentum 275–550 MeV/c is accompanied by the emission of a correlated neutron that carries a momentum roughly equal to and opposite from the initial proton momentum.

The BNL experiment did not measure the recoil protons. However, the ratio of probabilities of *pp* and *pn* SRCs has been estimated (21) using the result of Equation 28, yielding

$$P_{pp/pX} \leq \frac{1}{2}(1 - P_{pn/pX}) = 0.04^{+0.09}_{-0.04}. \qquad 29.$$

The above-mentioned JLab experiment (22, 23) made progress in verifying these results for the probabilities of *pn* and *pp* SRCs; the experiment detected both recoil protons and neutrons in the $^{12}\mathrm{C}(e, e'p, N_r)$ reaction. The experiment measured the fraction of $p_i > k_\mathrm{F}$ events in which there was a high-momentum, backward-angle-correlated proton or neutron:

$$R_{pp} = \frac{N\,[^{12}\mathrm{C}(e, e'p_f p_r)]}{N\,[^{12}\mathrm{C}(e, e'p_f)]} \quad \text{and} \quad R_{pn} = \frac{N\,[^{12}\mathrm{C}(e, e'p_f n_r)]}{N\,[^{12}\mathrm{C}(e, e'p_f)]}, \qquad 30.$$

where $N(\cdots)$ stands for the number of events.

After correcting for the effects of the detector acceptances and neutron efficiency, as well as estimating effects due to final-state interactions and the absorption of the produced nucleons, the

experiment found (22)

$$R_{pp} = (9.5 \pm 2)\% \quad \text{and} \quad R_{pn} = 96 \pm 22\%. \qquad 31.$$

R_{pp} was determined to be practically independent of p_i in the range 300–600 MeV/c, whereas R_{pn} was estimated for the whole $p_i > 300$ range. In relation to the BNL experiment, one observes remarkable agreement between R_{pn} and $P_{pn/pX}$ (from Equation 28), both of which represent the probability of finding a neutron in the pX correlation.

In the estimation of the probability of pp correlation in the JLab measurement, the experiment triggered only on forward $^{12}C(e, e'p)$ events. Thus, the probability of detecting pp pairs was twice that of detecting pn pairs, indicating that for single pp probability one should compare $P_{pp} = R_{pp}/2$ with the BNL's estimate of $P_{pp/pX}$—which, again, leads to very good agreement.

The above estimates lead to the following ratio of the probabilities of pp to pn 2N SRCs:

$$\frac{P_{pp}}{P_{pn}} = 0.056^{+0.021}_{-0.012}. \qquad 32.$$

This ratio confirms BNL's observation of the strong dominance of the pn component in NN SRCs.

The combined results from the BNL and JLab analyses are presented in **Figure 7*b***, which shows strong consistency between the results. The fact that these two experiments, employing different probes and covering different kinematics in momentum and energy transfer, obtained very similar results convincingly indicates that the observed phenomenon is a genuine property of the nuclear ground state.

3.6. Observation of Proton–Neutron Dominance in Heavy Nuclei

The experimental observation of pn dominance in the ^{12}C nucleus is understood on the basis of the dominance of the tensor interaction in the NN SRC. This fact itself indicates that the above-discussed experiments probed NN correlations at internal separations of $\lesssim$1 fm. Confidence in the validity of this conclusion is rather high because, as discussed in Section 2.3, the hypothesis of pn dominance leads to two new properties (Equations 16 and 17) of the high-momentum component of the nuclear wave function, which agree with the ab initio VMC calculations of light nuclei up to ^{11}B. Thus, one naturally expects that the ^{12}C nucleus, being next to ^{11}B, will still exhibit pn dominance.

If pn dominance is also valid for heavy nuclei, it will allow us to extrapolate our results to infinite nuclear matter (32), with rather striking implications for the properties of the superdense asymmetric nuclear matter found in the cores of neutron stars. However, it is not at all obvious that the phenomenon of pn dominance in NN SRCs will persist for heavy nuclei. For example, models in which the high-momentum component is generated from correlations between nucleons belonging to different nuclear shells predict that, for heavy nuclei, the contributions from higher orbitals (shells) will increase, thereby increasing the relative strength of NN SRCs with ($s = 0$, $t = 1$), ($s = 1$, $t = 1$), and ($s = 0$, $t = 0$) spin–isospin combinations (94). Such an effect can obscure the dominance of the $s = 1$ and $t = 0$ component of the short-range NN interaction. Unfortunately, one cannot unambiguously verify this question theoretically, as VMC calculations are currently applicable for light nuclei only. Other ab initio calculations that address heavy nuclei do not contain the short-range interaction component.

In this respect, experimental verification of pn dominance in heavy nuclei is significant. Such an analysis of experimental data from JLab has been performed (24), covering ^{12}C, ^{27}Al, ^{56}Fe, and ^{208}Pb nuclei. This analysis is similar to that discussed in the preceding section (22), except that it extracted the double ratios for nuclei A relative to ^{12}C: $[A(e, e'pp)/A(e, e'p)]/[^{12}C(e, e'pp)/^{12}C(e, e'p)]$. The

data analysis was constrained to the kinematics of $Q^2 \geq 1.5$ GeV^2, $x > 1.2$, and $300 < p_i < 600$ MeV/c, thereby minimally satisfying the condition of Equation 7. As in the previous analysis (22), corrections were made to account for final-state interactions and absorption effects. The final result of the analysis demonstrated that, at the 65% confidence level, *pn* dominance has been observed for all of the nuclei consistent with the estimate of Equation 32.

4. NEW DIRECTIONS: PROBING SHORT-RANGE CORRELATIONS IN DEEP-INELASTIC PROCESSES

Theoretically, as discussed in Section 2.5, one can use deep-inelastic processes to probe superfast quarks [$x = (AQ^2)/(2M_A q_0) > 1$] in nuclei. With the availability of high-energy electron beams, this represents a promising new technique for probing nuclear structure at short distances.

4.1. QCD Evolution of Superfast Quarks

One way to probe superfast quarks experimentally is in DIS from nuclei at $x > 1$ (25, 62). The verification that DIS experiments reached the superfast quark region comes from the extraction of nuclear partonic distributions that satisfy the QCD evolution equations. JLab's first attempt to reach the superfast region of the nuclear partonic distribution was made with a 6-GeV electron beam (95). In this experiment, due to the moderate values of $Q^2 \sim 7$ GeV^2, the greatest challenge was to account for the large higher twist, as well as finite mass effects. An interesting aspect of the new measurement was how it compared with earlier measurements from BCDMS/CERN (96) at $\langle Q^2 \rangle \sim 150$ GeV^2 and from CCFR/Fermilab (97) at $\langle Q^2 \rangle \sim 125$ GeV^2, which yielded mutually contradictory results.

The BCDMS Collaboration (96) measured the nuclear structure function $F_{2A}(Q^2, x)$ in DIS of 200-GeV muons from a ^{12}C target, extracting data for $\langle Q^2 \rangle = 61$–150 GeV^2 and $x = 0.85$–1.15. The per nucleon F_{2A} has been fitted in the following form:

$$F_{2A}(x, Q^2) = F_{2A}(x_0 = 0.75, Q^2) e^{-s(x-0.75)}, \qquad 33.$$

with the slope factor estimated as $s = 16.5 \pm 0.6$. Such an exponent corresponds to a very marginal strength of the high-momentum component of the nuclear wave function.

The CCFR Collaboration (97) extracted a per nucleon F_{2A} for an ^{56}Fe target measuring neutrino and antineutrino scattering in the charged-current sector for $\langle Q^2 \rangle = 125$ GeV^2 and $0.6 \leq x \leq 1.2$. This experiment obtained the slope of the x distribution in the form of Equation 33; the exponent was evaluated as $s = 8.3 \pm 0.7 \pm 0.7$. This result clearly contradicted the BCDMS result, as it required the strength of the high-momentum component of the wave function of the ^{56}Fe nucleus to be much too large. This strength was greater than the one deduced from quasi-elastic electroproduction in the $x > 1$ region (13, 18–20, 31, 32).

This contradiction could in principle be solved by the JLab experiment if its F_{2A} value could be related to the BCDMS and CCFR data by the QCD evolution equation. In the JLab experiment (95), the per nucleon structure functions F_{2A} were extracted in the Q^2 range of 6–9 GeV^2 for the ^{12}C target. Provided that these structure functions are corrected for finite target mass and higher-twist effects, they could be used as an input to the QCD evolution equation in order to relate them to the structure functions in a different Q^2 range. An important feature of the high-x kinematics is that, due to the negligible contribution from gluons, the evolution equation for F_{2A} at a given Q^2 is fully expressed through the input of the same structure function measured at

different Q^2 (98):

$$\frac{dF_{2A}(x,Q^2)}{d\log Q^2} = \frac{\alpha_s}{2\pi} 2\left[1+\frac{4}{3}\log\left(1-\frac{x}{A}\right)\right] F_{2,A}(x,Q^2) + \frac{4}{3}\int_{x/A}^{1}\frac{dz}{1-z}\left[\frac{1+z^2}{z}F_{2A}\left(\frac{x}{z},Q^2\right)-2F_{2A}(x,Q^2)\right]. \quad 34.$$

Figure 8*b* depicts the results of the evolution of the JLab value of F_{2A} to the Q^2 region of the BCDMS and CCFR experiments. Two of the curves correspond to the two different procedures of the extraction of the leading-twist part of the structure function that is used as an input to the evolution equation (Equation 34). In the first curve, the experimental F_{2A} is corrected for the finite target mass effects according to Reference 99 and parameterized for a fixed Q^2 value of 7 GeV^2 (for details, see Reference 95). In the second curve, the same JLab data were analyzed simultaneously for finite target mass and higher-twist effects. The finite target mass was accounted

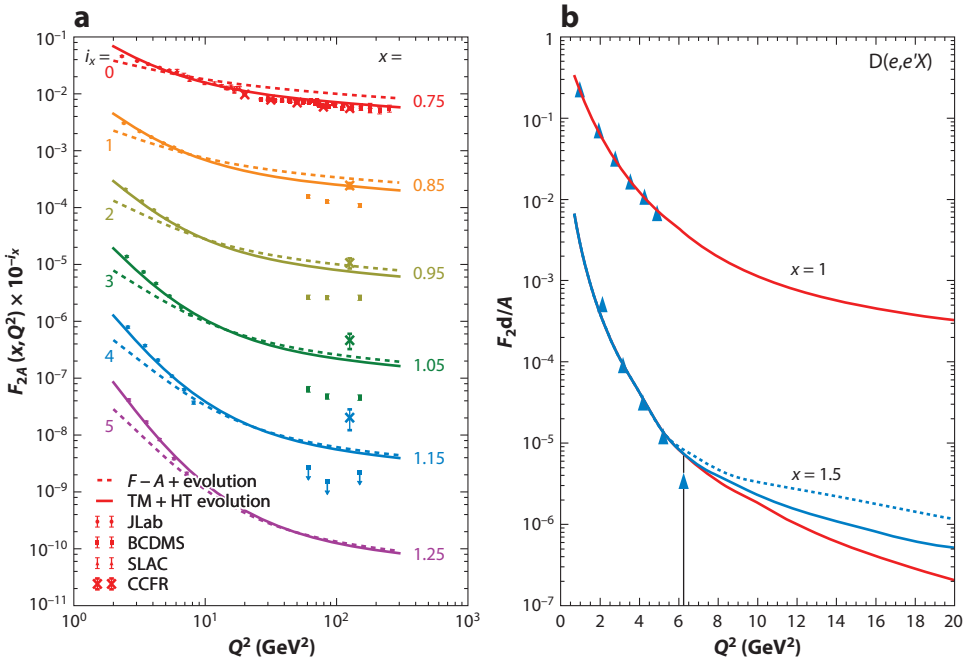

Figure 8

(*a*) Comparison between evolution equation results for the per nucleon F_{2A} of ^{12}C and experimental measurements. The JLab data are discussed in this review; details of the CCFR, BCDMS, and SLAC data can be found in Reference 95. The structure function is multiplied by 10^{-i_x} in order to separate the curves; the values of i_x for each x value are shown in the plot. Two curves correspond to the two different procedures for extracting the leading-twist part of the structure function that is used as an input to Equation 34. In the first curve, labeled $F - A +$ evolution, the experimental F_{2A} is corrected for the finite target mass effects according to Reference 99 and parameterized for a fixed Q^2 value of 7 GeV^2 (for details, see Reference 95). In the second curve, labeled TM + HT evolution, the same JLab data were analyzed simultaneously for finite target mass and higher-twist effects. (*b*) The deep-inelastic scattering structure function of the deuteron calculated with the convolution model with nucleon modification (*lower solid line*), with the six-quark model (*dotted line*), and with the hard gluon exchange model (*upper solid line*). These descriptions are related to the curves labeled $x = 1.5$. Data are from Reference 68.

for by employing the Nachtmann variable, $\xi = 2x/(1+\sqrt{1+Q^2/\nu^2})$, whereas higher-twist effects were separated through the parameterization of raw data in the form of the inverse powers of Q^2 (for details, see Reference 98).

As the comparisons with CCFR and BCDMS data in **Figure 8*b*** show, the two inputs predict very similar results in the high-Q^2 domain, agreeing better with the CCFR (the high-momentum nuclear component case) data for $x \leq 1.05$ and $Q^2 = 125$ GeV^2. For $x \sim 1.15$, the evolution of JLab's structure functions predict an F_{2A} value between the values obtained by CCFR and BCDMS. This result indicates that the actual strength of the high-momentum component of the nuclear wave function is likely larger than the BCDMS prediction and smaller than the CCFR prediction.

Again, we emphasize that the QCD evolution equation provides the best verification that the DIS process probed the superfast quarks in nuclei and provides a new tool for probing the strength of the high-momentum component of the nuclear wave function. By using the evolution equation to relate measurements in different Q^2 domains at $x > 1$, the new JLab 12-GeV data will clearly indicate whether the DIS has probed superfast quark distributions.

4.2. The Dynamics of the Generation of Superfast Quarks

As discussed above, the onset of the DIS regime in which superfast quarks are probed will result in a unique relation between structure functions F_{2A} measured at different Q^2 regions by the QCD evolution equations. However, these relations do not allow one to identify the dynamics responsible for the generation of superfast quarks in the nuclear medium. The discussion of the kinematics of DIS at $x > 1$ in Section 2.5 demonstrates that with an increase in Q^2 one can reach a domain of incredibly large internal momenta in the nucleus (**Figure 3*a***). In this respect, a primary question is whether the nucleonic degrees of freedom are still relevant for the description of the process. To address this issue, one can consider significantly different models of the generation of the superfast quarks, then investigate the feasibility of their experimental verification.

4.2.1. Convolution model. The first and most conventional approach is the convolution model, which assumes that the SRC of two or more nucleons in the nuclear medium provides sufficient initial momentum to the bound nucleon. These nucleons, in turn, supply the necessary momentum fraction to the superfast quarks. Within this scenario, the nucleons retain their degrees of freedom, but their structure may be strongly modified. Thus, in this case the nuclear structure function, F_{2A}, is expressed through the convolution of the structure function of the bound nucleon, $\tilde{F}_{2N}$, and the nuclear density matrix, $\rho_d^N(\alpha_i, p_T)$, as follows (25, 62, 65, 100):

$$F_{2A}(x, Q^2) = \sum_N \int_x^2 \rho_A^N(\alpha_i, p_T)\tilde{F}_{2N}\left(\frac{x}{\alpha}, Q^2\right)\frac{d\alpha}{\alpha}d^2p_T, \qquad 35.$$

where α represents the light-cone momentum fraction discussed above and p_T is the bound nucleon's transverse momentum. The bound nucleon structure function, $\tilde{F}_{2N}$, should account for the nuclear medium modifications, in agreement with the EMC effect (e.g., 25, 65, 100).

This model can be considered conventional because, except for the nuclear EMC effect, no nonnucleonic degrees of freedom are invoked in the calculation. In addition to the medium modification effects, which one expects to be proportional to the internal momentum of the bound nucleon, the short-range phenomena here enter through the $\rho_d^N(\alpha_i, p_T)$ function, which contains all of the effects of SRCs. The nuclear core effects enter through the *NN* potential, and one expects that for hard-core potentials they will result in the fast vanishing of $\tilde{F}_{2A}$ in the $x > 1$ region at large Q^2.

4.2.2. Six-quark model. The six-quark model is an extreme approach to the description of the evolution of superfast quarks in the nuclear medium in the region of $x \lesssim 2$. In this case, one assumes that short-range interactions between six quarks are responsible for the generation of superfast quarks. In the typical diagram, the six colinear quarks exchange five hard gluons, transferring the large part of the total momentum fraction to the superfast quark, which is subsequently probed by the virtual photon.

At asymptotically large Q^2 and the $x \to 2$ limit, one can deduce the x dependence of the structure function of nuclei, F_{2A}, using the general quark counting rule (101), according to which

$$F_{2A}(x)^{6q} \sim \left(1 - \frac{x}{2}\right)^{10}. \qquad 36.$$

Note that in this model one assumes that the high-momentum fraction carried by the superfast quark is achieved because of the mixing of all six quarks through the exchanges of hard gluons, thereby allowing a substantial contribution from the hidden color component of the six-quark system. In this case, however, the *NN* system is totally collapsed into a six-quark state, with complete disappearance of the nucleonic degrees of freedom and with no suppression due to the phenomenological hard-core repulsion. Thus, one expects a much softer x dependence of F_{2A} in the $x > 1$ region. In our numerical estimations, we use the parameterization of the six-quark model in Reference 63.

4.2.3. Hard single gluon exchange model. The hard single gluon exchange model considers an intermediate scenario in which the high-momentum fraction is supplied to the superfast quark not through the mixing of all six quarks involved in the *NN* system but rather by one hard gluon exchange between the two partons, which belong to two different nucleons. In this model, the only diagrams that contribute are those in which "communication" between two nucleons occurs through the single hard gluon exchange between two partons. Such diagram results in the convolution of two partonic distribution functions, one probed by the external photon and the other by the exchanged hard gluon:

$$F_{2A}(x) \approx N \left[\int \Psi_A(\alpha, p_T) \frac{d\alpha}{\alpha} \frac{d^2 p_T}{2(2\pi)^3}\right]^2 \qquad 37.$$
$$\times \int_0^1 \int_0^1 \left(1 - \frac{x}{y_1 + y_2}\right)^2 \Theta(y_1 + y_2 - x) f_N(y_1) f_N(y) dy_1 dy_2,$$

where f_N is the parton distribution function of the nucleon and y_1 and y_2 represent the momentum fractions of the partons, one from each nucleon, participating in the hard scattering. In this model, some of the effects of short-range repulsion will be present in the nonperturbative dynamics of the parton distribution function (PDF) of the nucleon. At asymptotically high Q^2 and the $x \to 2$ limit, the model has the parametric form of the six-quark model due to the $(1 - y)^3$ dependence of the nucleon PDFs.

In summary, we have presented three different scenarios of how superfast quarks can be generated in the *NN* system. The best way of determining which scenario is at play experimentally is using the deuteron target, because for heavy nuclei multinucleon SRCs might contribute strongly, masking effects arising from the *NN* interaction at the core.

Figure 8*b* presents the predictions of the above-discussed models for the structure function of the deuteron at $x = 1$ and $x = 1.5$. These estimates show a real possibility of discriminating between different scenarios of the interaction at core distances in future experiments with the 12-GeV JLab.

Extending the above discussion to heavy nuclei, we note that, in addition to the question of how the transition from the *NN* system to quark configuration occurs, one needs to address the question of 3*N* and higher-order SRCs. An interesting implication of the role of the 3*N* SRCs in the DIS regime is that if one considers the ratio of cross sections similar to that in the $1 < x < 2$ region of **Figure 4**, the plateau will disappear with the increase of Q^2. Such an effect is observed because, with an increase in Q^2 in the DIS regime, the internal momenta steeply increase at fixed x (Equation 23); as a result, even for $x < 2$, one should expect a substantial contribution due to 3*N* SRCs, which will disrupt the plateau observed experimentally in the quasi-elastic kinematics.

5. CONCLUSION AND OUTLOOK

We have reviewed recent progress in studies of SRCs in nuclei, driven by a series of high-energy experiments with proton and electron probes. We have demonstrated how the inclusive electronuclear processes in the $x > 1$ quasi-elastic region were able to both identify *NN* SRCs in nuclei and extract the parameter $a_2(A, Z)$, which characterizes the strength of *NN* SRCs in the high-momentum part of the nuclear wave functions. We have discussed the observation of an apparent correlation between the strength of the medium modification of partonic distributions in nuclei and the $a_2(A, z)$ factor of *NN* SRCs.

For triple coincidence experiments, we have reviewed the observed strong angular correlation between the constituents of *NN* SRCs and the strong dominance of the *pn* component in these correlations. The *pn* dominance is understood on the basis of the large tensor interaction in *NN* SRCs at distances $\lesssim$1 fm. We have reviewed the implication of this dominance on the properties of the high-momentum distribution of nucleons in nuclei, as well as recent observations that apparently are in agreement with these properties.

The current results on the physics of 3*N* correlations are rather inconclusive. We have shown that, in order to make a definitive probe of 3*N* correlations, one needs considerably higher values of Q^2, which can be obtained in upcoming experiments at JLab.

Finally, we have reviewed the new and promising direction of studying short-range properties of nuclei at core distances with DIS in the $x > 1$ region. We have reviewed the first such experiment completed at JLab and demonstrated its potential in verifying the validity of the QCD evolution equation for superfast quarks. We have also discussed the sensitivity of the cross section of inclusive scattering from superfast quarks to the particular mechanism of *NN* interactions at core distances. Future experiments at JLab, as well as at high-energy labs such as the LHC, J-PARC, and possibly the EIC, might provide significant new information about the dynamics of *NN* interactions at the core.

DISCLOSURE STATEMENT

The authors are not aware of any affiliations, memberships, funding, or financial holdings that might be perceived as affecting the objectivity of this review.

ACKNOWLEDGMENTS

During the writing of this manuscript, our good friend and coauthor Patricia Solvignon passed away. Though very young, Patricia had already had made quite an impact in the field of nuclear physics and had several approved experiments at JLab to measure the effects of short-range correlations in nuclei. In fact, Patricia was a spokesperson for several of the past and future JLab

experiments described herein. Patricia was a good friend and an outstanding scientist and will be sorely missed.

The writing of this review was supported by grants from the US Department of Energy, Office of Science, Office of Nuclear Physics, under contracts DE-SC0013615, DE-AC05-06OR23177, and DE-FG02-01ER-41172. We are thankful to our colleagues for collaboration and assistance in performing the above-described research in general and for help in preparation of this review in particular.

LITERATURE CITED

1. Machleidt R, Sammarruca F. *Phys. Scr.* 91:083007 (2016)
2. Lapikas L, et al. *Phys. Rev. C* 61:064325 (2000)
3. Jastrow R. *Phys. Rev.* 98:1479 (1955)
4. Bethe HA. *Annu. Rev. Nucl. Part. Sci.* 21:93 (1971)
5. Amado RD. *Phys. Rev. C* 14:1264 (1976)
6. Brueckner KA, Eden RJ, Francis NC. *Phys. Rev.* 98:1445 (1955)
7. Rock S, et al. *Phys. Rev. Lett.* 49:1139 (1982); Rock S, et al. *Phys. Rev. Lett.* 49:424 (1982)
8. Arnold RG, et al. *Phys. Rev. Lett.* 61:806 (1988)
9. Rock S, et al. *Phys. Rev. D* 46:24 (1992)
10. Day D, et al. *Phys. Rev. Lett.* 43:1143 (1979)
11. Rock S, et al. *Phys. Rev. C* 26:1592 (1982)
12. Day DB, et al. *Phys. Rev. Lett.* 59:427 (1987)
13. Frankfurt LL, Strikman MI, Day DB, Sargsian M. *Phys. Rev. C* 48:2451 (1993)
14. Royer D, et al. *Phys. Rev. C* 12:327 (1975)
15. Marchand C, et al. *Phys. Rev. Lett.* 60:1703 (1988); Marchand C, et al. Erratum. *Phys. Rev. Lett.* 60:2704 (1988)
16. Alanakian KV, et al. *Phys. At. Nucl.* 60:1069 (1997)
17. Alanakian KV, et al. *Phys. At. Nucl.* 61:207 (1998)
18. Egiyan KS, et al. *Phys. Rev. C* 68:014313 (2003)
19. Egiyan KS, et al. *Phys. Rev. Lett.* 96:082501 (2006)
20. Fomin N, et al. *Phys. Rev. Lett* 108:092502 (2012)
21. Piasetzky E, et al. *Phys. Rev. Lett.* 97:162504 (2006)
22. Shneor R, et al. *Phys. Rev. Lett.* 99:072501 (2007)
23. Subedi R, et al. *Science* 320:1476 (2008)
24. Hen O, et al. *Science* 346:614 (2014)
25. Frankfurt LL, Strikman MI. *Phys. Rep.* 160:235 (1988)
26. Seely J, et al. *Phys. Rev. Lett.* 103:202301 (2009)
27. Weinstein LB, et al. *Phys. Rev. Lett.* 106:052301 (2011)
28. Arrington J, et al. *Phys. Rev. C* 86:065204 (2012)
29. Sargsian MM, Abrahamyan TV, Strikman MI, Frankfurt LL. *Phys. Rev. C* 71:044615 (2005)
30. Schiavilla R, Wiringa RB, Pieper SC, Carlson J. *Phys. Rev. Lett.* 98:132501 (2007)
31. Sargsian MM. *Phys. Rev. C* 89:034305 (2014)
32. McGauley M, Sargsian MM. arXiv:1102.3973 [nucl-th] (2011)
33. Wiringa RB, Schiavilla R, Pieper SC, Carlson J. *Phys. Rev. C* 89:024305 (2014)
34. Ryckebusch J, Cosyn W, Vanhalst M. *J. Phys. G* 42:055104 (2015)
35. Boeglin WU, et al. *Phys. Rev. Lett.* 107:262501 (2011)
36. Hen O, Miller GA, Piasetzky E, Weinstein LB. arXiv:1611.09748 [nucl-ex] (2016)
37. Alvioli M, Ciofi degli Atti C, Morita H. *Phys. Rev. C* 94:044309 (2016)
38. Chen JW, Detmold W, Lynn JE, Schwenk A. arXiv:1607.03065 [hep-ph] (2016)
39. Boeglin W, Sargsian MM. *Int. J. Mod. Phys. E* 24:1530003 (2015)
40. Neff T, Feldmeier H, Horiuchi W. *Phys. Rev. C* 92:024003 (2015)
41. Ciofi degli Atti C. *Phys. Rep.* 590:1 (2015)

42. Cai BJ, Li BA. *Phys. Rev. C* 93:014619 (2016)
43. Furnstahl RJ, Hebeler K. *Rep. Prog. Phys.* 76:126301 (2013)
44. Weiss R, et al. arXiv:1612.00923 [nucl-th] (2016)
45. Ciofi degli Atti C, Mezzetti CB, Morita H. arXiv:1701.08211 [nucl-th] (2017)
46. Frankfurt LL, Strikman MI. *Phys. Rep.* 76:215 (1981)
47. Weinberg S. *Phys. Rev.* 150:1313 (1966)
48. Feynman RP. *Photon–Hadron Interactions*. Boulder, CO: Westview (1998)
49. Sargsian MM. *Int. J. Mod. Phys. E* 10:405 (2001)
50. Frankfurt LL, Sargsian MM, Strikman MI. *Phys. Rev. C* 56:1124 (1997)
51. Sargsian MM. *Phys. Rev. C* 82:014612 (2010)
52. Lepage GP, Brodsky SJ. *Phys. Rev. D* 22:2157 (1980)
53. Miller GA. *Prog. Part. Nucl. Phys.* 45:83 (2000)
54. Nogga A, Kamada H, Gloeckle W. *Nucl. Phys. A* 689:357 (2001)
55. Wiringa RB, Stoks VGJ, Schiavilla R. *Phys. Rev. C* 51:38 (1995)
56. Moniz EJ, et al. *Phys. Rev. Lett.* 26:445 (1971)
57. Artiles O, Sargsian MM. *Phys. Rev. C* 94:064318 (2016)
58. Frankfurt L, Sargsian MM, Strikman M. *Int. J. Mod. Phys. A* 23:2991 (2008)
59. Freese AJ, Sargsian MM, Strikman MI. *Eur. Phys. J. C* 75:534 (2015)
60. Sargsian MM, Abrahamyan TV, Strikman MI, Frankfurt LL. *Phys. Rev. C* 71:044614 (2005)
61. Aubert JJ, et al. *Phys. Lett. B* 105:315 (1981)
62. Sargsian MM, et al. *J. Phys. G* 29:R1 (2003)
63. Carlson CE, Lassila KE. *Phys. Rev. C* 51:364 (1995)
64. Sargsian MM. *Nucl. Phys. A* 782:199 (2007)
65. Melnitchouk W, Sargsian MM, Strikman MI. *Z. Phys. A* 359:99 (1997)
66. Cosyn W, Sargsian MM. *Phys. Rev. C* 84:014601 (2011)
67. Arrington J, et al. *Phys. Rev. C* 53:2248 (1996)
68. Arrington J, et al. *Phys. Rev. Lett.* 82:2056 (1999)
69. Arrington J, et al. *Phys. Rev. C* 64:014602 (2001)
70. Korover I, et al. *Phys. Rev. Lett.* 113:022501 (2014)
71. Egiyan KS, et al. *Phys. Rev. Lett.* 98:262502 (2007)
72. Ciofi degli Atti C, Simula S. *Phys. Rev. C* 53:1689 (1996)
73. Higinbotham DW, Hen O. *Phys. Rev. Lett.* 114:169201 (2015)
74. Gomez J, et al. *Phys. Rev. D* 49:4348 (1994)
75. Adams MR, et al. *Z. Phys. C* 65:225 (1995)
76. Amaudruz P, et al. *Nucl. Phys. B* 441:3 (1995)
77. Geesaman DF, Saito K, Thomas AW. *Annu. Rev. Nucl. Part. Sci.* 45:337 (1995)
78. Malace S, Gaskell D, Higinbotham DW, Cloet I. *Int. J. Mod. Phys. E* 23:1430013 (2014)
79. Higinbotham D, Miller GA, Hen O, Rith K. *CERN Cour.* 53N4:24 (2013)
80. Hen O, et al. *Int. J. Mod. Phys. E* 22:1330017 (2013)
81. Hen O, Piasetzky E, Weinstein L. *Phys. Rev. C* 85:047301 (2012)
82. Ducret J, et al. *Phys. Rev. C* 49:1783 (1994)
83. Blomqvist KI, et al. *Phys. Lett. B* 424:33 (1998)
84. Ulmer PE, et al. *Phys. Rev. Lett.* 89:062301 (2002)
85. Benmokhtar F, et al. *Phys. Rev. Lett.* 94:082305 (2005)
86. Rvachev M, et al. *Phys. Rev. Lett.* 94:192302 (2005)
87. Boeglin WU, et al. arXiv:1410.6770 [nucl-ex] (2014)
88. Passchier I, et al. *Phys. Rev. Lett.* 88:102302 (2002)
89. Mayer M. arXiv:1610.06109 [nucl-ex] (2016)
90. Mihovilovic M, et al. *Phys. Rev. Lett.* 113:232505 (2014)
91. Aclander JLS, et al. *Phys. Lett. B* 453:211 (1999)
92. Tang A, et al. *Phys. Rev. Lett.* 90:042301 (2003)
93. Yaron I, et al. *Phys. Rev. C* 66:024601 (2002)
94. Alvioli M, et al. *Phys. Rev. C* 87:034603 (2013)

95. Fomin N, et al. *Phys. Rev. Lett.* 105:212502 (2010)
96. Benvenuti AC, et al. *Z. Phys. C* 63:29 (1994)
97. Vakili M, et al. *Phys. Rev. D* 61:052003 (2000)
98. Freese AJ, Sargsian MM. arXiv:1511.06044 [hep-ph] (2015)
99. Schienbein I, et al. *J. Phys. G* 35:053101 (2008)
100. Sargsian MM, Simula S, Strikman MI. *Phys. Rev. C* 66:024001 (2002)
101. Brodsky SJ, Farrar GR. *Phys. Rev. Lett.* 31:1153 (1973)

Annual Review of Nuclear and Particle Science

Volume 67, 2017

Contents

Errata

An online log of corrections to *Annual Review of Nuclear and Particle Science* articles may be found at http://www.annualreviews.org/errata/nucl